Open access • Posted Content • DOI:10.1101/2021.10.18.464061

# The intestinal circadian clock drives microbial rhythmicity to maintain gastrointestinal homeostasis — Source link

Marjolein Heddes, Baraa Altaha, Yunhui Niu, Sandra Reitmeier ...+3 more authors

**Institutions:** Technische Universität München

**Published on:** 18 Oct 2021 - bioRxiv (Cold Spring Harbor Laboratory)

**Topics:** Circadian clock, CLOCK and Circadian rhythm

# The intestinal circadian clock drives microbial rhythmicity to maintain gastrointestinal homeostasis

Marjolein Heddes[1, 2,*], Baraa Altaha[1, 2,*], Yunhui Niu[1, 2], Sandra Reitmeier[1, 2], Karin Kleigrewe[3], Dirk Haller[1, 2], Silke Kiessling [1,2,4,†]

[†]Corresponding Author: Dr. Silke Kiessling, silke.kiessling@tum.de

*These authors contributed equally

[1] ZIEL - Institute for Food & Health, Technical University of Munich, 85354 Freising, Germany

[2] Chair of Nutrition and Immunology, Technical University of Munich, Gregor-Mendel-Str. 2, 85354 Freising, Germany

[3] Bavarian Center for Biomolecular Mass Spectrometry, Technical University of Munich, Gregor-Mendel-Str. 4, 85354 Freising, Germany

[4]Lead Contact

## Summary

**Diurnal (*i.e.*, 24-hour) oscillations of the gut microbiome have been described in various species including mice and humans. However, the driving force behind these rhythms remains less clear. In this study, we differentiate between endogenous and exogenous time cues driving microbial rhythms. Our results demonstrate that fecal microbial oscillations are maintained in mice kept in the absence of light, supporting a role of the host's circadian system rather than representing a diurnal response to environmental changes. Intestinal epithelial cell-specific ablation of the core clock gene *Bmal1* disrupts rhythmicity of microbiota. Targeted metabolomics functionally link intestinal clock-controlled bacteria to microbial-derived products, in particular branched-chain fatty acids and secondary bile acids. Microbiota transfer from intestinal clock-deficient mice into germ-free mice altered intestinal gene expression, enhanced lymphoid organ weights and suppressed immune cell recruitment. These results highlight the importance of functional intestinal clocks for circadian microbiota composition and function, which is required to balance the host's gastrointestinal homeostasis.**


## Introduction

Various physiological processes show 24-hour fluctuations. These rhythms are the expression of endogenous circadian (Lat. circa = about; dies = day) clocks that have evolved in most species [1] to facilitate anticipation of daily recurring environmental changes. In mammals, the circadian system includes a central pacemaker regulating sleep-wake behavior and orchestrating subordinated tissue clocks by humoral and neuronal pathways [2]. At the cellular level, these clocks consist of inter-regulated core clock genes [3] that drive tissue-specific transcriptional programs of clock-controlled genes (CCGs) [4]. Through these CCGs, circadian clocks regulate various aspects of physiology including metabolism, gastrointestinal transit

time (GITT), mucus secretion, antimicrobial peptide secretion, immune defense and intestinal barrier function (reviewed by [5-8]).

In mice, 10-15 % of gut bacteria undergo diurnal oscillations in their abundance influenced by meal timing, diet type and other environmental conditions [9-11]. Recently, we found similar rhythms in microbiota composition and function in population-based human cohorts [12]. Although functionality of the host's circadian system impacts microbial rhythmicity [10, 13, 14], it is unclear which tissue clocks contribute to this effect.

A balanced gut microbiome promotes health and microbial dysbiosis has been linked to metabolic diseases, colorectal cancer and gastrointestinal inflammation [12, 15-17]. Similar pathological consequences are associated with circadian rhythm disruption (reviewed by [18-20]), which also induces microbiota dysbiosis [10, 11, 13, 14, 21]. Consequently, we hypothesized that circadian regulation of microbiota composition and function may contribute to the host's GI health.

Here, we functionally dissect the circadian origin of microbiota oscillations in mice. We provide evidence that intestinal epithelial cell (IEC) clocks generate the majority of gut microbial rhythms and their metabolic products, particularly short-chain fatty acids (SCFAs) and bile acids (BAs). Transfer of microbiota from IEC clock-deficient mice in germ-free (GF) wild type hosts directly indicate the consequences of microbiota arrhythmicity on the gastrointestinal homeostasis. Thus, we identify a mechanistic link between IEC clocks, gut bacteria rhythms and their functions through transfer experiments, showing the importance of rhythmic microbiota for host physiology.

## Results

### Rhythms in microbiota are generated endogenously by the circadian system

Diurnal rhythms in microbiota composition and function have been demonstrated in animal models and in humans [9-12]. However, it has not been demonstrated whether these rhythms

are a response to rhythmic external cues (*Zeitgebers)*, such as the light-dark cycle, or are generated by endogenous clocks [22] and, thus, persist when the organism is placed in an environment devoid of timing cues. To address this question, we compared fecal microbiota rhythms of the same wild-type mice kept in a rhythmic 12-hour light/12-hour dark (LD) cycle and constant darkness (DD) for two weeks (**Fig. 1A**). Host-driven rhythmic factors, which might influence microbiota composition, such as locomotor activity, food intake as well as total GI transit time (GITT), did not differ between light conditions (**Suppl. Fig 1A-D**). 16S rRNA profiling of fecal samples revealed clustering based on sampling time points in both light conditions (**Fig. 1B**). Generalized UniFrac distances (GUniFrac) quantification identified rhythmicity in both light conditions, although with a 40% reduced amplitude in DD ($p = 0.0033$, **Fig. 1C**). Importantly, 24-hour rhythms of species richness and Shannon effective number of species found in LD persisted in DD, supporting their circadian origin (**Fig. 1D**). Rhythms were also preserved in DD on phylum level with the two most dominant phyla Bacteroidetes and Firmicutes, oscillating in antiphase (**Fig. 1E, F**). Although microbiota composition is commonly analyzed by relative abundance, rhythmicity of highly abundant taxa may mask oscillations of small microbial communities, as previously demonstrated in fecal samples collected in LD [13]. Therefore, using synthetic DNA spikes, we performed relative quantification of the copy number of 16S rRNA genes according to Tourlousee et al. [23], from here on referred to as 'quantitative analysis'. With both approaches, highly abundant phyla and families, including *Lachnospiraceae* and *Muribaculaceae*, showed comparable circadian rhythmicity in LD and DD (**Fig. 1F; Suppl. Fig. 1E**). Few families, such as *Prevotellaceae* showed significant diurnal (LD), but no circadian (DD) rhythmicity, suggesting that their rhythms are regulated by the environmental LD cycle (**Suppl. Fig. 1E**). After removal of low-abundant taxa (mean relative abundance > 0.1%; prevalence > 10%), the remaining 580 zOTUs displayed robust and comparable 24-hour oscillations in both light conditions, independent of the analysis (**Fig. 1G, H; Suppl. Fig. 1F-I**). The wide distribution of peak abundances, e.g.,

bacteria peaking during the day (mainly belonging to *Muribaculaceae*) and during the night (*Lachnospiraceae*) (**Fig. 1G, H; Suppl. Fig. 1F-H**), suggests that different microbial taxa dominate different daytimes. Importantly, about ¾ of all identified zOTUs were found to significantly oscillate in LD and about 80 % of these diurnal zOTUs remained rhythmic in DD (**Fig. 1G, H, Suppl. Fig. 1F-H, Suppl. table 1**), suggesting that their rhythmicity is generated by the circadian system. Rhythmicity of the majority of zOTUs (e.g. the genera *Alistipes*, *Oscillibacter* and *Fusimonas*) identified by relative analysis was further validated by quantitative analysis (73 % in LD, 58 % in DD) **(Suppl. Fig. 1 I, J).** Although most zOTUs were found to be controlled by the circadian system, less than 20 % of zOTUs (e.g. the genera *Alloprevotella* and *Aneaeroplasma*) lost rhythmicity in DD (**Fig. 1G**; **Suppl. Fig. 1K**), indicating the rhythmicity of these taxa depends on rhythmic environmental cues. Altogether, these data suggest that the diurnal rhythmicity found in ¾ of all zOTUs examined is generated by the endogenous circadian system.

## Robust microbial rhythms during simulated shift work

Alterations in gut microbiota communities as well as disrupted diurnal oscillation in specific taxa, such as *Faecalibacterium*, have been reported in shift work and jetlag conditions in human and mouse studies [10, 24]. In our study, external light conditions only mildly effect microbial rhythms (**Fig. 1**), thus prompting us to determine microbial rhythmicity under simulated shift work (SSW) conditions. SSW mice were exposed to 8-hour shifts of the LD cycle every 5$^{th}$ day for a minimum of 6 weeks and compared to littermates kept in stable LD conditions (**Fig. 2A**). Total activity, food intake and GITT were comparable between both cohorts (**Suppl. Fig. 2A-C**). However, altered activity profiles and advanced activity onsets were observed in SSW mice (**Fig. 2A, Suppl. Fig. 2A**) reflecting the transient state of chronodisruption observed after such rapid LD phase shifts [25]. Microbial profiles oscillated in both light conditions and rhythms of major phyla were preserved in SSW **(Fig. 2B,-E).** Heatmaps of bacterial abundances over

the course of the 24-hour day illustrated rhythmic patterns in both light conditions for both relative and quantitative analyses (**Fig. 2F, Suppl. Fig. 2D**). Importantly, the majority of rhythmic zOTUs (56 % relative abundance, 49 % quantitative analysis) including the genera *Alistipes, Duncaniella, Odoribacter and Fusimonas,* maintained rhythmicity during SSW (**Fig. 2G, H; Suppl. Fig. 2D, E**). A small amount of zOTUs (19%), including *Lactobacillus johnsonii* and *Eubacterium* became arrhythmic under SSW conditions (**Suppl. Table 1**). Interestingly, SSW advanced the peak abundance of microbial oscillations by about 3 hours, which was visible on all taxonomic levels (**Fig. 2C-G; Suppl. Fig. 2D, E**). An advanced food intake behavior during SSW might have contributed to the phase advance observed in microbial rhythms, because the feeding time was shown to influence the phasing of microbiota rhythmicity [10, 11]. Thus, we set out to determine microbiota rhythmicity in the absence of both *Zeitgeber* food and light by collecting feces from starved mice during the 2$^{nd}$ day in DD (**Fig. 3A**). Clustering according to collection time points was significant in both feeding conditions, although starvation altered microbial composition (**Fig. 3B**). Microbiota diversity became arrhythmic in the absence of food (**Fig. 3C**). However, rhythms persisted in the two dominant phyla, highly abundant families, including *Muribaculaceae* and *Lachnospiraceae* and the majority of zOTUs (**Fig. 3D-F**). Of note, circadian food intake behavior enhanced the amount of rhythmic zOTUs by 17%, including the genera *Alistipes* and *Faecalibacterium rodentium* and specific members of *Lachnospiraceae* (**Fig. 3F-G**), in accordance with previous report [11]. Nevertheless, circadian rhythms of highly abundant microbial taxa belonging to *Muribaculaceae* and *Ruminococaceae* maintained under starving conditions (**Fig. 3 H**).

Together, these data show that although rhythms in gut bacteria are slightly influenced by environmental light and food conditions, intrinsic factors are the dominant drivers of circadian microbiota fluctuations.

## The intestinal circadian clock controls microbiota composition and function

An important role of the host clock on diurnal microbiota fluctuation has previously been suggested based on experiments on mice with clock dysfunction in all tissues under LD conditions [10, 13, 14]. The GI tract represents an important interface for cross-talk between IECs, bacteria and their metabolites [26] and thus might likely be involved in controlling microbiota composition. To identify the circadian origin of microbial rhythmicity, we used mice with IEC-specific deletion of the essential core clock gene *Bmal1* (*Bmal1*$^{IEC-/-}$). The rhythmic activity, food intake behavior as well as GITT and stool weight of *Bmal1*$^{IEC-/-}$ mice did not differ from control littermates, reflecting a functional central pacemaker (**Suppl. Fig. 3A-E**). Arrhythmic core clock gene expression in the jejunum, cecum and proximal colon, in contrast to rhythms in the liver, confirmed intestine-specific clock ablation in *Bmal1*$^{IEC-/-}$ mice (**Suppl. Fig. 3F**). Rhythmic genes relevant for host-microbe crosstalk, in particular *Tlr2*, *Muc2*, *Nfil3* and *Hdac3* [27-32] lost rhythmicity in *Bmal1*$^{IEC-/-}$ mice (**Suppl. Fig. 3G**). In line with this, microbiota composition differed significantly between *Bmal1*$^{IEC-/-}$ mice and controls ($p = 0.037$) and circadian rhythmicity in community diversity (species richness) observed in control mice was abolished in *Bmal1*$^{IEC-/-}$ mice (**Fig. 4A, B**). Quantitative analysis revealed loss of rhythmicity of Firmicutes in *Bmal1*$^{IEC-/-}$ mice ($p = 0.313$), although, oscillation in relative abundance of the major phyla was found in both genotypes, (**Fig. 4C**). In accordance to results obtained from whole-body clock-deficient mice [13], IEC-specific loss of *Bmal1* decreased the quantitative abundance of both phyla, which was not visible in relative data sets (**Fig. 4C**). Similarly, rhythmicity observed in the relative abundance of families, including *Lachnospiraceae* and *Ruminococcaceae*, was abolished performing quantitative analysis (**Suppl. Fig. 3H).** Furthermore, dramatically disrupted circadian oscillations of *Bmal1*$^{IEC-/-}$ mice in both relative and quantitative analyses was observed on the level of all 580 identified zOTUs illustrated by heatmaps (**Fig. 4D, E**). Of note, in *Bmal1*$^{IEC-/-}$ mice the phase of remaining microbial oscillations was delayed using quantitative analysis (**Fig. 4D, E**). Based on both analyses more than 60 % of fecal zOTUs, which account for more than two-third of bacterial

abundance, underwent circadian oscillation in controls (**Fig. 4D, E**). Around two-third of circadian zOTUs lost rhythmicity upon IEC-specific *Bmal1* deficiency in both analyses (**Fig. 4D, E, Suppl. Table 1**). zOTUs which lost rhythmicity in *Bmal1*$^{IEC-/-}$ mice shared between both relative and quantitative analysis belong predominantly to the families *Lachnospiraceae* and *Ruminococcaceae* of the phylum Firmicutes **(Fig. 4F, Suppl. Fig. 3I).** The genera *Lactobacillus, Muribaculum*, *Anaerotignum* and *Fusimonas* are among the taxa which lost rhythmicity in *Bmal1*$^{IEC-/-}$ mice and significantly differed in their abundance between genotypes (**Fig. 4F, G, Suppl. Fig. 3I**). Although the majority of zOTUs was under intestinal clock control, rhythmicity of around 20% of zOTUs (e.g. *Lactobacillus animalis* and *Pseudoflavonifractor*) persisted in *Bmal1*$^{IEC-/-}$ mice (**Fig. 4D, E, Suppl. Table 1**). To address whether these remaining rhythms were driven by the rhythmic food intake behavior observed in *Bmal1*$^{IEC-/-}$ mice kept under ad libitum conditions in DD (**Fig. 4**), microbiota rhythmicity in *Bmal1*$^{IEC-/-}$ mice was analyzed in feces from starved mice during the 2$^{nd}$ day in DD (as described in **Fig. 3A**). Indeed, in *Bmal1*$^{IEC-/-}$ mice half of the remaining rhythms under *ad libitum* conditions were abolished upon starvation, for examples bacteria belonging to *Oscillibacter* and *Pseudoflavonifractor* (**Suppl. Fig. 4A, B**). Consequently, these results suggest that IEC clocks are the dominant driver for circadian oscillations of gut bacteria.

## Intestinal clock-controlled microbial functions balance gastrointestinal homeostasis.

To address the potential physiological relevance of microbial oscillations, PICRUST 2.0 analysis was performed on intestinal-clock controlled zOTUs. Loss of microbial rhythmicity in *Bmal1*$^{IEC-/-}$ mice was reflected in assigned pathways involved in sugar- and amino acid metabolism, vitamin biosynthesis and relevant for fatty acid (FA) metabolism such as β-oxidation, FA elongation and short-chain FA (SCFA) fermentation (**Fig 5A, B**). This prompted us to test the functional connection between intestinal clock-driven microbial rhythmicity and metabolic homeostasis. Indeed, Procrustes analyses (PA) identified an association between

intestinal clock-controlled zOTUs and SCFA concentrations measured by targeted metabolomics ($p = 0.001$) (**Fig. 5C**). The level of valeric acid ($p = 0.04$) and low-abundant branched-chain fatty acids (BCFAs) ($p = 0.01$), including isovaleric, isobutyric, 2-methylbutyric differed between genotypes, although the amount of total and highly abundant SCFAs were comparable (**Fig 5D**). Nevertheless, concentrations of SCFAs negatively correlated with the relative abundance of intestinal clock-driven taxa, mainly belonging to the family *Muribaculaceae* of the phylum Bacteroidetes (**Fig. 5E**). Positive significant correlations with multiple SCFAs, in particular BCFAs, where found with zOTUs belonging to the phylum Firmicutes, including the SCFA producers *Lachnospiraceae* and *Ruminococcaceae* (**Fig. 5E**) [33]. Similar to the results observed for SCFAs, associations were found between intestinal clock-controlled zOTUs and BAs levels ($p = 0.04$, **Fig. 5F**). Positive correlations with primary BAs and negative correlations with secondary BAs were observed with several intestinal clock-controlled taxonomic members mainly belonging to Firmicutes (**Fig. 5G**). For example, DHLCA and 7-sulfo-CA negatively correlated with *Oscillibacter* and *Eubacterium* (**Fig. 5G, H**). In addition, almost half of the measured BAs differed among genotypes and, BAs, such as the conjugated primary BA, TCDA, and secondary BA, 7-sulfo-CA, lost rhythmicity in Bmal1$^{IEC-/-}$ mice (**Fig. 5I-M**). Interestingly, most alterations were observed for secondary BAs (**Fig. 5L**), which were linked to various GI diseases (reviewed by [34]). In summary, these results indicate that deletion of intestinal clock function causes loss of rhythmicity in the majority of bacterial taxa and alters microbial functionality.

## Transfer of arrhythmic intestinal clock-controlled microbiota disturbs GI homeostasis

To further test the physiological relevance of intestinal clock-driven rhythmic microbial composition and its functionality on host physiology, GF C57BL/6 mice were colonized with cecal content from *Bmal1*$^{IEC-/-}$ or control mice (n=4) (**Fig. 6A**). Interestingly, ~76 % of bacteria from the control and *Bmal1*$^{IEC-/-}$ donor, were transferred into the recipients (**Suppl. Fig. 5A**).

Reduced richness was observed in mice after microbiota transfer (**Suppl. Fig. 5B**), in line with previous reports [35]. Interestingly, microbiota composition of recipient wild-type hosts significantly differed depending on the genotype of the donor (**Fig. 6B; Suppl. Fig. 5 C, D**). Most of the transferred taxa belonged to Firmicutes, whose rhythmicity strongly depends on a functional intestinal clock, whereas abundances in Bacteroidetes were highly suppressed (**Fig. 6C; Suppl. Fig. 5C**). Importantly, lack of rhythmicity was transferred to mice receiving microbiota from *Bmal1*$^{IEC-/-}$ mice (**Fig. 6D, E**). In particular rhythmicity of zOTUs belonging to e.g. *Alistipes*, shown to be driven by the gut clock (**Fig. 3P**) and maintained circadian rhythmicity in the host after transfer from control donors, lack rhythmicity in mice receiving microbiota from *Bmal1*$^{IEC-/-}$ mice (**Fig. 6E**). Altered expression of intestinal clock genes in jejunum and colon was observed after transfer of arrhythmic microbiota in comparison to recipientin mice receiving rrhythmic microbiota (**Suppl**. **Fig. 5E**). Moreover, the expression of genes involved in host-microbe interaction, including *Arg2* and *Tlr4,* significantly differ depending on the genotype of the donor (**Fig. 6F**). For example, arrhythmic microbiota induced the expression of *Il33, NfkB* both known to be involved in intestinal inflammatory responses [36, 37] and reduced the expression of *Ang4 and Hdac3* (**Fig. 6F**) which integrate microbial and circadian cues relevant for inflammatory and metabolic intestinal functions [30, 38, 39], Forman et al., 2012, Hardbower et al., 2016).

Although mesenteric lymph nodes and colon weights of mice associated with arrhythmic microbiota were undistinguishable from controls, and histology scores were unaffected, we noticed a significant increase in spleen and jejunum weight (**Fig. 6G),** indicating a role of microbial rhythmicity on host intestinal homeostasis, **(Suppl. Fig. 5F, G)**. Indeed, transfer of arrhythmic microbiota altered immune cell recruitment to the lamina propria. For example, an increase in dendritic cells (CD11c+) was detected in the small intestine whereas recruitment of

T cells (CD3+CD4+, CD3+CD8+) and dendritic cells (CD11c+) to the lamina propria of the colon was decreased (**Fig. 6H, Suppl. Fig. 5H**).

Together, these results indicate that deletion of intestinal clock function caused loss of rhythmicity in the majority of bacterial taxa, alters microbial functionality and resets the host's intestinal homeostasis.

## Discussion

Diurnal microbial oscillations in the major phyla and families have previously been demonstrated in humans and mice by us and others [9-13]. Here we provide evidence that rhythmicity of the majority of these taxa persists even in the absence of external timing cues, demonstrating the endogenous origin of fecal bacterial circadian rhythms. In contrast, strongly attenuated microbial rhythms in cecal and ileal content were found in mice kept in DD [40]. Differences in the amount and type of oscillating microbes between studies may be explained by variations in microbiota composition of the mouse lines, microbial ecosystem between facilities and niches within the GI tract. Moreover, we detected largely sustained microbiota oscillations during SSW, indicating that circadian rhythmicity of microbiota composition is rather robust against environmental disturbance. These results are in contrast to work by Thaiss et al. illustrating impairment of diurnal microbiota oscillations in mice exposed to chronic jetlag [10]. However, the majority of zOTUs that maintained rhythmicity in this study (e.g. the genera *Alistipes* and *Roseburia)* were undetectable in previous studies [10, 21, 41]. Nevertheless, disrupted rhythmicity as well as a reduced abundance of specific taxa (e.g. the genera *Eubcaterium*) identified in this study confirmed previous reports [10, 21, 41]. The comparability between studies may be impacted by methodological differences, such as differences in the 16S rRNA variable target gene region used for amplicon sequencing (here: V3-V4, [40]: V4, [10]: V1-V2, [21].: V1-V3, [41]: Metatranscriptome) as well as the sampling intervals (here: 3h/day, [40]: 6h/day, [10]: 4h/day).

Our results obtained from constant environmental conditions suggest that circadian microbiota regulation is primarily rooted in host or bacterial intrinsic circadian mechanisms. Indeed, using IEC-specific *Bmal1*-deficient mice, we provide the first demonstration for a dominant role of intestinal clocks in driving circadian microbiota composition. Lack of *Bmal1* in IECs led to dramatic loss of microbiota rhythmicity, predominantly belonging to the phylum Firmicutes, which was independent of whether relative or quantitative analyses was used. Of note, both microbiota analyses in this study did not always yield identical results, highlighting the importance of both analyses to interpret circadian microbiota composition. Microbiota composition is commonly analyzed by relative abundance; yet this analysis may exaggerate microbial rhythmicity due to masking by highly abundant taxa [13]. Arrhythmicity in taxa (e.g. *Lactobacillaceae, Odoribacteraceae* and *Lachnospiraceae)* was previously documented in mice lacking *Bmal1* or *Per1/2* tissues-wide [10, 13]. Loss of oscillations of the same taxa among others was observed in $Bmal1^{IEC-/-}$ mice, identifying the IEC-clock to generate rhythmicity of these bacteria. Most of the remaining bacteria which were unaffected by IEC clock-deficiency, lost circadian rhythmicity upon starvation. Some of these taxa have previously been reported to be influenced by food availability [11]. A prominent role for the timing of food intake on microbial rhythmicity was frequently suggested [9-11]. However, we demonstrate that even in the absence of food, rhythmicity of dominant bacteria persisted, thus rhythmic food intake is not required to drive microbiota oscillations. Accordingly, in mice supplied with constant intravenous parenteral nutrition cecal microbiota composition oscillated [9]. Importantly, the majority of microbial rhythms was abolished in $Bmal1^{IEC-/-}$ mice even though these mice show rhythmic food intake behavior. These results further highlight that IEC clocks are the dominant driver whereas environmental changes as well as food-intake are mere modulators of microbial rhythms.

Mechanisms how intestinal clocks regulate microbiota rhythms likely involve local epithelial-microbe interactions and immune functions, including pattern recognition receptors, such as Toll-Like Receptors (TLRs), Aryl hydrocarbon receptors and nuclear receptors as well as antimicrobial peptide production and mucus secretion, all previously found to oscillate diurnally [29, 30, 42]. Accordingly, we found IEC clocks to be essential for rhythmic expression of related genes, such as *Tlr2*, *Ang4*, *Muc2*, *Nfil3* and *Hdac3,* which are engaged in bidirectional microbe-host communication. For example, IEC-specific deletion of *Hdac3* or loss of *Tlr2* altered microbial composition and influenced intestinal homeostasis [43, 44]. Furthermore, *Muc2* can affect microbiota composition by allowing bacteria to metabolize mucin glycans [45], which through cross-feeding affects the abundance of other microbial taxa [46]. However, future studies are required to functionally investigate intestinal clock mechanism controlling microbiota composition.

Circadian disruption due to life style has been correlated to microbiota dysbiosis and human health (reviewed by [47]). Recently, we found a functional link between arrhythmicity of microbiota and the development of obesity and T2D [12]. Here we demonstrate intestinal-clock dependent rhythmicity of taxa involved in SCFA fermentation, such as *Lachnospiraceae, Ruminococcaceae* and *Odoribacteraceae*, lactate acid producing bacteria e.g. *Lactobacillaceae*, mucus foragers, such as *Muribaculaceae, Rickenellaceae* and *Lachnospiraceae* [33, 48, 49]. Moreover, taxa capable to convert bile acids (BAs), including *Lactobacillus*, *Clostridium* and *Eubacterium* [50] are regulated by intestinal circadian clocks. Consequently, IEC clocks likely influence microbiota function. Indeed, functional analysis based on 16S rRNA gene data revealed pathways such as SCFA fermentation, amino-acid and carbohydrate metabolism are associated to intestinal clock-controlled taxa. Many among the identified pathways were shown to diurnally oscillate in healthy individuals, to lose rhythmicity in clock deficient mice, and are associated with host's health [10, 12, 51]. Targeted metabolite

316 analysis further confirmed that arrhythmicity in intestinal clock-controlled taxa is reflected in
317 alterations of key metabolites involved in lipid signaling pathways such as SCFAs and BAs.
318 Both of these microbiota-related metabolites are known to diurnally oscillate and impact,
319 among others host immune and metabolic functioning [9, 52-56]. Notably, high levels of
320 secondary BAs, e.g. DCAs and HDCAs identified in *Bmal1*$^{IEC-/-}$ mice, were also found in
321 subjects with metabolic disorders including obesity and T2D [57-60]. Moreover, TUDCA lost
322 circadian rhythmicity in *Bmal1*$^{IEC-/-}$ mice and was found to ameliorate insulin sensitivity in both
323 obese mice and humans [61, 62]. In addition, accumulation of BAs within the host has been
324 associated with several GI diseases. For example, increased levels of the sec BA DCA and
325 taurine-conjugated Bas (TDCA), was also observed in patients with GI cancer, inflammatory
326 bowel disease (IBD) and UC ([63] and reviewed by [34]). These results support the hypothesis
327 that a functional intestinal clock balances GI health by driving microbial function.
328 Transfer experiments provide direct evidence for the physiological relevance of intestinal
329 clock-controlled microbiota and their functions. Microbial rhythmicity and arrhythmicity
330 depending on the donor genotype induced molecular and physiological changes in the healthy
331 hosts. Notably, a functional intestinal clock in recipients seems to require longer than 5 weeks
332 to restore microbial rhythmicity, suggesting strong microbe-host clock interactions. Indeed this
333 was supported by altered clock gene expression in recipients receiving arrhythmic microbiota
334 and is in accordance with a report indicating a role of microbial rhythmicity in programing host
335 transcriptome rhythmicity [64]. Additionally, microbial metabolite production, e.g. SCFAs and
336 BAs, in recipients may have influenced intestinal clock functions, since a direct impact on
337 rhythmicity in intestinal epithelial cells and subsequent metabolic responses in the host has been
338 provided previously [9, 45].
339 Transfer of arrhythmic microbiota from intestinal clock-deficient mice altered several genes
340 involved in inflammation, antimicrobial peptide production and intestinal epithelial functioning
341 including *Tnf-α, Tlr2, Lgr5, Ffar2, Hdac3* and *Nf-kB* [36-38, 65-68]. Changes in the expression

of these genes due to reception of arrhythmic microbiota might have caused the observed immune phenotype in recipients. For example, *Tlr2* senses the presence of microbe-associated molecular patterns and is capable to regulate the host's immune system against pathogenic infiltration by regulating *Tnf-α* cytokine production of CD8+ T-cells [69, 70]. Moreover, *Hdac3* and *Il33* also plays an important role in microbe-host crosstalk [43, 71]. Mouse models lacking HDAC3 show high susceptibility to DSS-induced inflammation, partly by activation of NF-kb, the latter also observed in our mouse model [43, 72] . Consequently, altered regulation of *Tlr2*, *Tnf-α, Hdac3*, and *IL-33* expression observed in mice receiving arrhythmic microbiota, likely disturbed gastrointestinal homeostasis. Indeed, enhanced lymphoid tissues weight and suppressed recruitment of T-cell and dendritic cell populations to the lamina propria within the colon was found in GF mice receiving arrhythmic microbiota from intestinal clock-deficient mice. Immune cell recruitment represents an important aspect in the gastrointestinal immune defense (reviewed by [73]. Consequently, we provide the first evidence that intestinal clock-controlled rhythmic gut bacteria are crucial for a balanced intestinal immune homeostasis, and likely influence the immune response to pathogens, infection and inflammation.

Taken together, a functional intestinal clock represents a key element to maintain metabolic health by driving rhythmicity of gut bacteria and microbial products. Since intestinal clock functions effect bacterial taxa associated to metabolic health and microbiota required for a balanced immune defense, it remains to be studied whether arrhythmicity of intestinal clock-controlled taxa is causal for the development of gastrointestinal diseases. In the scope of previous associations of arrhythmic microbiota and their products with T2D and IBD [12, 74], our data highlight the relevance to further investigate intestinal clock mechanisms driving bacterial rhythmicity for human health.

## ADDITIONAL INFORMATION (CONTAINING SUPPLEMENTARY INFORMATION LINE (IF ANY) AND CORRESPONDING AUTHOR LINE)

## ACKNOWLEDGEMENT

The Technical University of Munich provided funding for the ZIEL Institute for Food & Health, animal facility support, technical assistance and support for 16S rRNA gene amplicon sequencing. Johanna Bruder provided assistance with animal experiments and preliminary data collection.

## AUTHOR CONTRIBUTIONS

SK conceived and coordinated the project. MH, BA and YN performed mouse experiments and fecal samples collection. BA, MH and YN provided tissue samples and performed gene expression analysis. SK and MH analyzed activity and food intake behavior. MH, BA, SR and SK performed 16S rRNA gene sequencing and bioinformatics analysis. BA and MH analyzed predicted microbial functionality. YN performed FACS analyses. MH and KK performed targeted metabolomics and data analysis. SK supervised the work and data analysis. SK and DH secured funding. MH, BA, DH and SK wrote the manuscript. All authors reviewed and revised the manuscript. MH and BA contributed equally to this work.

## FUNDING

SK was supported by the German Research Foundation (DFG, project KI 19581) and the European Crohn´s and Colitis Organisation (ECCO, grant 5280024). SK and DH received funding by the Funded by the Deutsche Forschungsgemeinschaft (DFG, German Research Foundation) – Projektnummer 395357507 – SFB 1371).

## CORRESPONDING AUTHOR

Correspondence to Dr. Silke Kiessling, Chair of Nutrition and Immunology, Technical University of Munich, Gregor-Mendel-Str. 2, 85354 Freising, Germany.

## DECLARATION OF INTEREST

The authors declare no competing interests.

# FIGURE LEGENDS

## Figure 1 Fecal microbial rhythms persist in constant darkness

(A) Representative actogram of control (*Bmal1*$^{IECfl/f}$) mice exposed to light-dark (LD) cycle and two weeks of constant darkness (DD). Fecal sampling times are indicated by red arrows. (B) Beta-diversity principal coordinates analyses plot (PCoA) of fecal microbiota based on generalized UniFrac distances (GUniFrac) and separated for individual time points in LD (left) and DD (right) conditions and its quantification over time relative to ZT1/CT1 (C). (D) Diurnal (LD) and circadian (DD) profiles of alpha-diversity. (E) Dendrogram of microbiota profiles based on GUniFrac in LD and DD conditions. Taxonomic composition at phylum and family level for each sample is shown as stacked bar plots around the dendrogram. The blue inner circle indicates the sampling time. (F) Diurnal (LD) and circadian (DD) profiles of the relative (left)) and quantitative abundance (right) of phyla. (G) Heatmap depicting the relative abundance of 580 zOTUs (mean relative abundance > 0.1%; prevalence > 10%). Data are normalized to the peak of each zOTU and ordered by the peak phase in LD conditions. Pie-charts at the right indicate the amount of rhythmic (blue) and arrhythmic (grey) zOTUs identified by JTK_Cycle (outer circle) and their cumulative abundance (inner circle). (H) Significance and amplitude of rhythmic and arrhythmic zOTUs (left) and phase distribution (right) in LD and DD based on relative analysis. Dashed line indicates p = 0.05, JTK_Cycle. Significant rhythms are illustrated with fitted cosine-regression; data points connected by straight lines indicate no significant cosine fit curves (p > 0.05) and thus no rhythmicity. Significant baseline differences are illustrated with an asterisk. LD (light-blue) and DD (dark-blue). n = 6 mice/time point/light condition. Data are represented as mean ± SEM. Significance $p \leq 0.05$.

## Figure 2 Robust rhythms of microbiota during simulated shift work

(A) Representative actogram of a control mouse in 12-hour light/12-hour dark (LD) and under simulated shift work (SSW) condition. Tick marks represent running wheel activity; yellow and grey shadings represent light and darkness respectively; red arrows indicate fecal sample collection time points. (B) Diurnal profile of GUniFrac distances over time relative to ZT1. (C-E) Diurnal profile of the relatve abundance of major phyla. (F) Heatmap depicting the relative abundance of 473 zOTUs (mean relative abundance > 0.1%; prevalence > 10%). Data are normalized to the peak of each zOTU and ordered by the peak phase in LD conditions. (G) Significance and amplitude of rhythmic and arrhythmic zOTUs (top) and phase distribution (bottom) in LD and SSW. Dashed line indicates p = 0.05, JTK_Cycle. (H) Pie-charts indicate the amount of rhythmic (blue, yellow, red) and arrhythmic (grey) zOTUs identified by JTK cycle (outer circle) and their cumulative abundance (inner circle). Significant rhythms are illustrated with fitted cosine-regression; data points connected by straight lines indicate no significant cosine fit curves (p > 0.05) and thus no rhythmicity. Significant baseline differences are illustrated with an asterisk. Significant phase shifts ($p \leq 0.05$) are indicated with the number of hours of phase shift. LD (grey) and SSW (red). n = 4-5 mice/time point/light condition. Data are represented as mean ± SEM.

## Figure 3 Food intake behaviour marginally masks microbiota rhythmicity

(A) Schematic illustration of experiment design. (B) Beta-diversity PCoA plots based on GUniFrac distances of microbiota stratified by individual time points in Ad libitum (left) and starvation (right). (C) Circadian profiles of alpha-diversity. (D) Beta-diversity principal

coordinates analyses plot (PCoA) of fecal microbiota based on generalized UniFrac distances (GUniFrac) stratified by feeding condition. (E) Circadian profiles of the relative abundance of the major phyla of fecal microbiota. (F) Heatmap depicting the relative abundance of 507 zOTUs (mean relative abundance > 0.1%; prevalence > 10%). Data are normalized to the peak of each zOTU and ordered by the peak phase in Ad libitum condition. The relative abundance of zOTUs showing diurnal rhythmicity in Ad libitum and starvation. Significance and amplitude of rhythmic and arrhythmic zOTUs (top) and phase distribution (bottom). Dashed line indicates p = 0.05, JTK_Cycle. G-H: Circadian profile of relative abundance of zOTUs of fecal microbiota. Significant rhythms (cosine-wave regression) are illustrated with fitted cosine-wave curves; data points connected by straight lines indicate no significant cosine fit curves ($p > 0.05$) and thus no rhythmicity. Significant baseline differences are illustrated with an asterisk. Ad libitum (black) and starvation (purple). n = 9-11-5 mice/time point/light condition. Data are represented as mean ± SEM.

## Figure 4 The intestinal circadian clock drives circadian microbiota composition

(A) Beta-diversity principal coordinates analyses plot (PCoA) of fecal microbiota based on generalized UniFrac distances (GUniFrac) stratified by genotype. (B) Circadian profile of alpha diversity. (C) Circadian profile of relative (top) and quantitative (bottom) abundance of the major phyla. (D-E) Heatmap depicting the relative abundance (D) and quantitative abundance (E) of 580 zOTUs (mean relative abundance > 0.1%; prevalence > 10%). Data are normalized to the peak of each zOTU and ordered by the peak phase of control mice. Pie-charts at the right indicate the amount of rhythmic (colored) and arrhythmic (grey) zOTUs identified by JTK_Cycle (outer circle) and their cumulative abundance (inner circle) based on relative (D) and quantitative (E) analysis. Significance and amplitude of rhythmic and arrhythmic zOTUs (top) and phase distribution (bottom) in controls and *Bmal1*$^{IEC-/-}$ mice is depicted on the right of the heatmaps. Dashed line indicates p = 0.05, JTK_Cycle. Bar charts in (F) represent the zOTUs abundance comparison between control and *Bmal1*$^{IEC-/-}$ color coded according to the pie charts. Box and bar plots illustrate the alteration in relative abundance and fold change of gut controlled zOTUs in the fecal samples with examples depicted in (G). Significant rhythms are illustrated with fitted cosine-regression; data points connected by straight lines indicate no significant cosine fit curves ($p > 0.05$) and thus no rhythmicity. significant baseline differences are illustrated with an asterisk. Control (green) and *Bmal1*$^{IEC-/-}$ (red). n = 5-6 mice/time point/genotype. Data are represented as mean ± SEM. Significance $p \leq 0.05$.

## Fig. 5 Metabolic functioning of intestinal clock-controlled bacteria

(A) Heatmap of MetaCyc Pathways predicted using PICRUST2.0 on intestine clock-controlled zOTUs rhythmic in control (left) and arrhythmic in *Bmal1*$^{IEC-/-}$ (right) mice and (B) showing significant differences in abundance between genotypes. Pathways are colored according to their sub-class. (C) Procrustes analyses (PA) of fecal microbiota and SCFA levels. The length of the line is proportional to the divergence between the data from the same mouse. (D-E) SCFA concentrations in feces (D) and their Spearman correlation ($p \leq 0.05$ and $R \leq -0.5$; red or $R \geq 0.5$; blue) (E) with gut controlled bacteria taxa. (F) PA as described in (C) with fecal bile-acid (BA) levels. (G) Spearman correlation of BA concentrations with intestine clock-controlled microbiota and examples (H). Total (I), deconjugated primary (J), conjugated primary (K) and secondary (L) fecal BAs levels and their circadian profiles (M). Significant rhythms are illustrated with fitted cosine-regression; data points connected by straight lines indicate no significant cosine fit curves ($p > 0.05$) and thus no rhythmicity. n =5-6 mice/time point/genotype. Control (green) and *Bmal1*$^{IEC-/-}$ (red). Data are represented as mean ± SEM. Significance * $p \leq 0.05$, ** $p \leq 0.01$, *** $p \leq 0.001$, **** $p \leq 0.0001$ (One-way ANOVA).

BSCFA=branched-chain fatty acids. Cholic acid (CA), a-Muricholic acid (aMCA), b-Muricholic acid (bMCA), Taurocholic acid (TCA), Taurochenodeoxycholic acid (TCDCA), Tauroursodeoxycholic acid (TUDCA), Taurohyodeoxycholic acid (THDCA), Taurolithocholic acid (TLCA), Taurodeoxycholic acid (TDCA), Tauro-a-Muricholic acid (TaMCA), Glycochenodeoxycholic acid (GCDCA), Glycocholic acid (GCA), Deoxycholic acid (DCA), Lithocholic acid (LCA), y-Muricholic acid (y-MCA), 12-Dehydrocholic acid (12-DHCA), 12-Ketolithocholic acid (12-keto-LCA), 3-Dehydrocholic acid (3-DHCA), 6-Ketolithocholic acid (6-keto-LCA), 7-Dehydrocholic acid (7-DHCA), 7-Sulfocholic acid (7-sulfo-CA), Allocholic acid (ACA), Cholic acid-7ol-3one (CA-7ol-3one), Ursocholic acid (UCA), Dehydrolithocholic acid (DHLCA), Hyodeoxycholic acid (HDCA), Murideoxycholic acid (MDCA), Ursodeoxycholic acid (UDCA).

## Figure 6 Intestinal clock-controlled rhythmic microbiota is essential for intestinal homeostasis

(A) Schematic illustration of transfer experiments with mixture of cecal microbiota obtained from Control and *Bmal1*$^{IEC-/-}$ donors (n=4) into 10 weeks old germ-free BL6 wild-type recipient mice for the duration of 6 weeks. (B) PCoA plot of GUniFrac distances of donor (CT13) and recipient mice (n=6/8/genotype/time point) after 5 weeks of transfer. (C) Diurnal profiles of fecal microbiota at phylum level. (D) Heatmap depicting the relative abundance of zOTUs ordered by their cosine-regression peak phase according to the recipient controls. On the left the first 2 columns indicate donor zOTU abundance. (E) Diurnal profile of relative abundance of example zOTUs. (F) Relative gene expression of *Tlr4, Arg2, Ang4, Tnfa, Il33, Nfkb, Hdac3, Lgr5* in the proximal colon of recipient mice. (G) Organ weights of recipient mice after receiving control (green) or *Bmal1*$^{IEC-/-}$ (red) cecal microbiota. (H) Frequency of CD3+CD4+, CD3+CD8+, CD11c+ cells in jejunum and colon. Significant rhythms are illustrated with fitted cosine-regression; data points connected by straight lines indicate no significant cosine fit curves ($p > 0.05$) and thus no rhythmicity. n = 6 mice/time point/genotype. Data are represented as mean ± SEM. Significance * $p \leq 0.05$, ** $p \leq 0.01$, *** $p \leq 0.001$, **** $p \leq 0.0001$.

# SUPPLEMENTAL FIGURE LEGENDS

*Supplement Figure 1 Diurnal and circadian rhythms in behavior and microbiota composition*

(A) Diurnal (LD) and circadian (DD) total wheel-running activity profiles and 24-h summary (B). Total daily food intake (C) and gastro-intestinal transit time (GITT) (D). (E) Diurnal and circadian profile of relative (left) and quantitative (right) abundance of the major family of fecal microbiota. (F) Heatmap depicting the quantitative abundance of 580 zOTUs (mean relative abundance > 0.1%; prevalence > 10%). Data are normalized to the peak of each zOTU and ordered by the peak phase in LD conditions. (G) Pie-charts indicate the amount of rhythmic (blue) and arrhythmic (grey) zOTUs identified by JTK_Cycle. (H) Significance and amplitude of rhythmic and arrhythmic zOTUs (left) and phase distribution (right) in LD and DD based on quantitative analysis. Dashed line indicates p = 0.05, JTK_Cycle. (I) Pie-charts indicating percentage of overlap in rhythmic (green) and arrhythmic (grey) zOTUs between relative (top) and quantitative (bottom) analyses in LD (left) and DD (right) conditions. (J) Taxonomic tree of circadian zOTUs shared by both relative and quantitative analyses. Taxonomic ranks are from phylum (outer dashed ring), family (inner ring) to genera (middle, color coded according to phylum) indicated by individual branches. (K) Box and bar plots illustrate the alteration in relative abundance and fold change between LD and DD of zOTUs, which lost rhythmicity in DD. Significant rhythms are illustrated with fitted cosine-regression; data points connected by straight lines indicate no significant cosine fit curves (p > 0.05) and thus no rhythmicity. LD (light-blue) and DD (dark-blue). n = 6 mice/time point/conditions. Data are represented as mean ± SEM.

*Supplement Figure 2 Quantitative microbiota composition in mice exposed to simulated shift work (SSW)*

(A) Diurnal total wheel-running activity profiles (left) and 24-h summary (middle, right). Total daily food intake (B) and gastro-intestinal transit time (GITT) (C). (D) Heatmap depicting the quantitative abundance of 473 zOTUs (mean relative abundance > 0.1%; prevalence > 10%). Data are normalized to the peak of each zOTU and ordered by the peak phase of control mice. Pie-charts on the right indicate the amount of rhythmic (colored) and arrhythmic (grey) zOTUs identified by JTK_Cycle. (E) Profiles of zOTU relative abundance of 4-5 mice/time point in LD (black) and SSW (red) conditions. Significant rhythms are illustrated with fitted cosine-regression; data points connected by straight lines indicate no significant cosine fit curves (p > 0.05) and thus no rhythmicity. Significant baseline differences are illustrated with an asterisk (# $p \leq 0.05$). n = 4-5 mice/time point/genotype. Data are represented as mean ± SEM.

*Supplement Figure 3 Characterization of rhythmic behavior and microbial profiling of Bmal1$^{IEC-/-}$ mice*

(A) Representative actogram in LD and DD conditions of *Bmal1*$^{IECfl/fl}$ controls and *Bmal1*$^{IEC-/-}$ mice. (B) Activity profile of *Bmal1*$^{IEC-/-}$ and control mice in light-dark (LD) cycle (upper left) and the quantification of circadian activity (upper middle) and the period in DD (upper right) as well as food intake diurnal profile (lower left) and its average (lower middle), and food intake circadian profile (lower right). (C) Circadian profile of fecal production (top) and GITT (bottom) of *Bmal1*$^{IEC-/-}$ and control mice. Expression profiles of core clock genes (D) and clock-controlled genes (E). (F) Circadian profiles at family level of relative abundance (left) and quantitative abundance (right) of control and *Bmal1*$^{IEC-/-}$ mice. (G) Taxonomic tree of fecal

circadian gut clock controlled microbiota uniquely rhythmic in control mice in both relative and quantitative analyses. Taxonomic ranks are from phylum (outer dashed ring), family (inner ring highlighted) to genera (middle, color coded according to phylum) which are indicated by the individual branches. Significant rhythms are illustrated with fitted cosine-regression or fitted harmonic-regression; data points connected by straight lines indicate no significant cosine fit curves ($p > 0.05$) and thus no rhythmicity. *Bmal1*$^{IEC-/-}$ (red) and control (green). n = 5-6 mice/time point/genotype. Data are represented as mean ± SEM. Significance $p \leq 0.05$. Significant baseline differences are illustrated with an asterisk (# $p \leq 0.05$).

*Supplement Figure 4 Microbiota profiling in Bmal1*$^{IEC-/-}$ *mice during starvation*

(A) Heatmap illustrating microbiota loosing rhythmicity after starvation in *Bmal1*$^{IEC-/-}$ mice. Data are normalized to the peak of each zOTU and ordered by the peak phase in *ad libitum* condition. (B) Circadian profiles of the relative abundance of example zOTUs masked by the food-intake behavior. Significant rhythms are illustrated with fitted cosine-regression; data points connected by straight lines indicate no significant cosine fit curves ($p > 0.05$) and thus no rhythmicity. Significant baseline differences are illustrated with an asterisk (# $p \leq 0.05$). n = 9-12 mice/time point/condition. Data are represented as mean ± SEM.

*Supplement Figure 5. Arrhythmic microbial transfer to germ-free mice*

(A) Percentage of zOTUs transferred (black) and not transferred (grey) into recipient mice. (B) Richness of donor (n=4 mixture) and recipient samples collected at CT13/ZT13. Taxonomic binning of microbiota from donor and recipient mice at CT13/ZT13 at phyla (C) and family (D) level. (E) Clock gene expression measured at CT13 in Jejunum (top) and proximal colon (bottom) of recipient mice 6 weeks after microbiota transfer of control or *Bmal1*$^{IEC-/-}$ mice. (F) Organ weights of recipient mice after receiving control or *Bmal1*$^{IEC-/-}$ cecal microbiota. (G) Cross section of proximal colon along with the histological scoring of proximal colon and jejunum of germ-free mice after receiving control or *Bmal1*$^{IEC-/-}$ cecal microbiota. (H) Immunofluorescence staining of CD3 (green), E-cadherin (red) and Dapi (blue) of proximal colon of germ-free mice after receiving control or *Bmal1*$^{IEC-/-}$ cecal microbiota. * $p< 0.05$, ** $p< 0.01$, *** $p<0.001$, **** $p<0.0001$ (two-way ANOVA). Significant rhythms in circadian profiles are illustrated with fitted cosine-wave curves (cosine-wave regression, $P \leq 0.05$).

# METHODS

## Ethics Statement

Experiments were conducted at Technical University of Munich in accordance with Bavarian Animal Care and Use Committee (TVA ROB-55.2Vet-2532.Vet_02-18-14).

## Mouse models

### *Bmal1$^{IEC\ tg/wt}$ and Bmal1$^{IECfl/fl}$ mouse generation*

Male epithelial intestinal epithelial cell-specific *Bmal1* knock-out *(Bmal1fl/fl* x Villin CRE/wt; referred to as *Bmal1$^{IEC-/-}$*) mice and their control littermates (*Bmal1fl/fl* x Villin wt/wt ; referred to as *Bmal1$^{fl/fl}$*) on a genetic C57BL/6J background were generated as previously described [75]. Breeding was performed by crossing *Bmal1fl/fl* x Villin CRE/wt with *Bmal1fl/fl* x Villin wt/wt. Unless otherwise stated, mice were kept in LD 12:12 cycles (300 lux), with lights turned on at 5am (*Zeitgeber* time (ZT0) to 5pm (ZT12)). All mice were single housed at the age of 8 weeks in running wheel-equipped cages with ad libitum access to chow and water and under specific-pathogen free (SPF) conditions according the FELASA recommendation. In order to minimize cage-related bias in microbiota composition [76], littermates and litters of comparable age from as few as possible breeding pairs and cages were selected.

## Behavior analysis and fecal sample collection

All male mice, unless stated otherwise, were individually housed in cages with running wheels. Handling and activity measurements during experiments were performed as described [77]. Wheel-running activity was analyzed using ClockLab software (Actimetrics). The last 10-14 days of each condition were used to determine the period (tau, calculated using a $X^2$ periodogram and confirmed by fitting a line to the onsets of activity), the duration of the active period (alpha), the amount of activity and the subjective day/night activity ratio (where the subjective day under DD conditions is the inactive period between the offset of activity and the

onset of activity and the subjective night is the active period between the onset of activity and the offset of activity).

### *Light-dark (LD) and constant darkness (DD) conditions*

Male *Bmal1*$^{IEC-/-}$ and their control littermates *Bmal1*$^{IECfl/fl}$ were maintained under LD cycle for 2 weeks (age 8-10 weeks), switched to a DD cycle for 2 more weeks (age 10-12 weeks), kept in constant light (LL) for an additional 2 weeks (age 12-14w) and finally returned back to LD till the age of 18-20 weeks before sacrifice. Average daily food intake was measured over 5 consecutive days in the second week of the above indicated light conditions. Of note, Fecal sample collection in darkness was performed after adjusting for each mouse's individual free-running period (**Suppl. Fig. 3A**). For example, the activity period varied by ~0.5 hours per day within mice of the same genotype and consequently accumulates to a ~7 hours phase difference between individual mice after 2 weeks in DD.

### *Simulated shift work (SSW)*

10-week-old *Bmal1*$^{IEC-/-}$ male mice and *Bmal1*$^{IECfl/fl}$ control littermates were subjected to SSW conditions for at least 6 weeks. Mice were exposed to 100lux light intensity and shifted every 5$^{th}$ days by 8 hours. On day 1 of the jet lag, the lights-off time (ZT12) was shifted from 5 pm to 9 am (phase advance paradigm) and from 9 am to 5 pm (phase delay paradigm). Using a short day protocol, we defined day 1 as the first advanced dark period as defined previously [25].

### *Food deprivation*

11-week-old *Bmal1*$^{IEC-/-}$ male mice with *ad libitum* food intake were used for fecal sample collection. At the age 12-13 weeks the mice were starved as illustrated in (**Suppl. Fig. 4A**). Briefly, food was removed at CT1 on the 1$^{st}$ day in DD. Fecal samples collection started at CT13 on the 2$^{nd}$ day in DD (after 13 hours of starvation) till CT10 (after 34 hours of starvation).

### *Food intake pattern and analysis*

The diurnal food intake pattern of individually housed mice was recorded using an automated monitoring system (TSE LabMaster Home Cage Activity, Bad Homburg, Germany) at the age of 10-12 weeks. Mice were habilitated for 3 days. Then data were collected for a full 24-hours profile at the 4$^{th}$ day. Cumulative food intake was recorded through high precision balances connected to the food baskets. Food basket weight were summed up in 1 min intervals. Total food intake was calculated as 1$^{st}$ derivative of cumulative food intake and consumption was summed up at intervals of 1 hour. One-minute intervals where the weight loss was directly followed by a similar weight gain in food baskets within a period of 3 minutes were excluded. Circadian food intake of individually housed mice was recorded in the second day of darkness by weighing the food every 3 hours.

### *Complete gastrointestinal transit time*

Complete GI transit time (GITT) was measured by administering natural carmine red (6%, SigmaAldrich) dissolved in 0.5% methylcellulose (Sigma-Aldrich) by gavage (100ul) according to [78]. 16-18 week-old male *Bmal1*$^{IEC-/-}$ and *Bmal1*$^{fl/fl}$ mice were starved 6h prior to gavage. Time of gavage was considered T0. In case of presence, fecal pellets were taken out of the cage every 10 minutes and checked for red color. GITT was registered as the time between T0 and the time of presence of carmine red in the fecal pellets.

### *Tissue collection*

All animals were sacrificed by cervical dislocation at the age of 18-20 weeks in the second day of darkness at the indicated circadian times (CT) or in LD12:12 conditions, in 4 hour intervals starting at 1 hour after lights off (ZT1). In constant darkness samples were collected at the indicated time points used for control mice in LD. Eyes were removed prior to tissue dissection. Tissues were harvested and snap frozen on dry ice and stored in -80 degrees.

## Gene expression analysis (qRT-PCR) Quantitative real-time PCR

RNA was extracted from snap frozen tissue samples with Trizol reagent. cDNA was synthesized from 1000ng RNA using cDNA synthesis kit Multiscribe RT (Thermofischer Scientific). qPCR was performed in a Light Cylcer 480 system (Roche Diagnostiscs, Mannheim, Germany) using Universal Probe Library system according to manufacturer's instructions. For genes expression the following primers and probes were used: Brain and Muscle ARNT-Like 1 *(Bmal1)* F 5'-ATTCCAGGGGGAACCAGA-' R 5'-GGCGATGACCCTCTTATCC-3' Probe 15, Period 2 *(Per2)* F 5'-TCCGAGTATATCGTGAAGAACG-3' R 5'- CAGGATCTTCCCAGAAACCA-3' probe 5, Nuclear receptor subfamily 1 group D member 1 *(Reverbα)* F 5'-AGGAGCTGGGCCTATTCAC-3' R 5'-CGGTTCTTCAGCACCAGAG-3' probe 1, Toll-like receptor 2 *(Tlr2)* F- 5'-GGGGCTTCACTTCTCTGCTT-3' R 5'-AGCA TCCTCTGAGATTTGACG-3' probe 50, Angiogenin 4 *(Ang4)* F 5'-CCCCAGTTGGAGGAAAGC-3' R 5'-CGTAGGAATTTTTCGTACCTTTCA-3' probe 106, Mucin 2 *(Muc2)* F 5'- GGCAGTACAAG AACCGGAGt-3' R 5'-GGTCTGGCAGTCCTCGAA-3' probe 66, Histone Deacetylase 3 *(Hdac3)* F 5'- GAGAGGTC CCGAGGAGAAC-3' R 5'-CGCCATCATAGAACTCATTGG-3' probe 40, Tumor necrosis factor alpha *(Tnfa)* F 5'- TGCCTATGTCTCAGCCTCTTC-3' R 5'-GAGGCCATTTGGGAACTTCT-3' probe 49, Leucine Rich Repeat Containing G Protein-Coupled Receptor 5 *(Lgr5)* F 5'- CTTCACTCGGTGCAGTGCT-3' R 5'-CAGCCAGCTACCAAATAGGTG-3' probe 60, Toll like receptor *(Tlr4)* F 5'-GGACTCTGATCATGGCACTG -3' R 5'-CTGATCCATGCATTGGTAGGT-3' probe 2, Nuclear factor kappa-light-chain-enhancer of activated B cells *(Nfkb)* F 5'-CCCAGACCGCAGTATCCAT -3' R 5'- GCTCCAGGTCTCGCTTCTT-3' probe 47. RNA abundance was normalized to the housekeeping gene Elongation factor 1-alpha *(Ef1a)* F 5'-GCCAAT TTCTGGTTGGAATG-3' R 5'-GGTGACTTTCCATCCCTTGA-3' probe 67. For

692 Interleukin33 (*Il33*) gene was used syber green to run the gene using the following primer F 5'-
693 GAACATGAGTCCCATCAAAG -3' R 5'- CAGCTGGTTATCTTTTACTCC -3' and RNA
694 abundance was normalized to the housekeeping gene *Ef1a* F 5'- GCCAAT
695 TTCTGGTTGGAATG-3' R 5'-GGTGACTTTCCATCCCTTGA-3'.

696 **High-Throughput 16S Ribosomal RNA (rRNA) Gene Amplicon Sequencing Analysis**

697 Genomic DNA was isolated from snap-frozen fecal pellets according to a modified protocol of
698 (Godon et al., 1997) as previously described [12]. DNA NucleoSpin gDNA columns (Machery-
699 Nagel, No. 740230.250) were used for DNA purification. In a two-step PCR the V3-V4 region
700 (using the primers 341F-ovh and 785r-ov) of the 16S rRNA gene was amplified from 24 ng
701 DNA. After pooling, the multiplexed samples were sequenced on an Illumina HiSeq in paired-
702 end mode (2x250 bp) using the Rapid v2 chemistry, in accordance with [12]. Two negative
703 controls, consisting of DNA stabilizer without stool, were used for every 45 samples to control
704 for artifacts and insure reproducibility. High-Quality sequences of read counts > 5000 were
705 used for 16s rRNA data analysis. Reads FASTQ files were consequently processed using an in-
706 house developed NGSToolkit (Version Toolkit 3.5.2_64 ) based on USEARCH 11 [79]. A trim
707 score of 5 was used on the 5' end and 3'end for the R1 and R2 read followed by chimera removal
708 [80] using the FASTQ mergepair script of USEARCH [79]. Quality filtered reads were merged,
709 deduplicated, clustered and a denoised clustering approach was applied to generate zOTUs [79,
710 81]. Taxonomic assignment was performed with the EZBiocloud database (Yoon et al., 2017).
711 Data was further analyzed with the R-based pipeline RHEA [82]. Phylogenetic trees are
712 generated by a maximum likelihood approach, which was performed on an alignment generated
713 by MUSCLE with the software MegaX [83]. Trees were visualized and annotated with the use
714 of the online tool EvolView (http://www.evolgenius.info/evolview/) [84]. Spike-in of 12
715 artificial DNA standards mimicking 16S rRNA genes (a surrogate for bacterial numbers) were
716 used to determine the quantitative copy numbers of rRNA genes per gram of fecal sample

between samples. Briefly, the same amount of artificial DNA (6ng) was added to each weighted fecal sample before DNA extraction. After sequencing as described above, FASTQ files were mapped against the spike FASTA sequences (using bowtie2), removing the spike reads and generating a new FASTQ file. By comparing the spike sequencing reads to the fecal bacterial reads; we calculate the quantitative number of 16S rRNA gene copies per gram of sample. The copy number of 16S rRNA gene is proportional to the number of bacteria present in a sample. Thus, this approach enables estimation of microbial abundances relative between samples, suitable for comparative analysis according to Tourlousse et al. (2016).

## Targeted metabolite analyses

### *Sample preparation for targeted metabolite analyses*

Approximately 20 mg of mouse fecal pellet was weighed in a 2 mL bead beater tube (CKMix 2 mL, Bertin Technologies, Montigny-le-Bretonneux, France) filled with 2.8 mm ceramic beads. 1 mL of methanol-based dehydrocholic acid extraction solvent (c=1.3 µmol/L) was added as an internal standard for work-up losses. Fecal samples were extracted with a bead beater (Precellys Evolution, Bertin Technolgies) supplied with a Cryolys cooling module 3 times each for 20 seconds with 15 seconds breaks in between at 10.000 rpm.

### *Targeted bile acid measurement*

20 µL of isotopically labelled bile acids (ca. 7 µM each) were added to 100 µL of sample extract. Targeted bile acid measurement was performed using a QTRAP 5500 triple quadrupole mass spectrometer (Sciex, Darmstadt, Germany) coupled to an ExionLC AD (Sciex, Darmstadt, Germany) ultrahigh performance liquid chromatography system. A multiple reaction monitoring (MRM) method was used for the detection and quantification of the bile acids. An electrospray ion voltage of −4500 V and the following ion source parameters were used: curtain gas (35 psi), temperature (450 °C), gas 1 (55 psi), gas 2 (65 psi), and entrance potential (−10 V). The MS parameters and LC conditions were optimized using commercially available

742 standards of endogenous bile acids and deuterated bile acids, for the simultaneous
743 quantification of selected 28 analytes. For separation of the analytes a 100 × 2.1 mm, 100 Å,
744 1.7 µm, Kinetex C18 column (Phenomenex, Aschaffenburg, Germany) was used.
745 Chromatographic separation was performed with a constant flow rate of 0.4 mL/min using a
746 mobile phase consisted of water (eluent A) and acetonitrile/water (95/5, v/v, eluent B), both
747 containing 5 mM ammonium acetate and 0.1% formic acid. The gradient elution started with
748 25% B for 2 min, increased at 3.5 min to 27% B, in 2 min to 35% B, which was hold until 10
749 min, increased in 1 min to 43% B, held for 1 min, increased in 2 min to 58% B; held 3 min
750 isocratically at 58% B, then the concentration was increased to 65% at 17.5 min, with another
751 increase to 80% B at 18 min, following an increase at 19 min to 100% B which was hold for 1
752 min, at 20.5 min the column was equilibrated for 4.5 min at starting. The injection volume for
753 all samples was 1 µL, the column oven temperature was set to 40 °C, and the auto-sampler was
754 kept at 15 °C. Data acquisition and instrumental control were performed with Analyst 1.7
755 software (Sciex, Darmstadt, Germany) as previously described [85]. BAs measured are Cholic
756 acid (CA), a-Muricholic acid (aMCA), b-Muricholic acid (bMCA), Taurocholic acid (TCA),
757 Taurochenodeoxycholic acid (TCDCA), Tauroursodeoxycholic acid (TUDCA),
758 Taurohyodeoxycholic acid (THDCA), Taurolithocholic acid (TLCA), Taurodeoxycholic acid
759 (TDCA), Tauro-a-Muricholic acid (TaMCA), Glycochenodeoxycholic acid (GCDCA),
760 Glycocholic acid (GCA), Deoxycholic acid (DCA), Lithocholic acid (LCA), y-Muricholic acid
761 (y-MCA), 12-Dehydrocholic acid (12-DHCA), 12-Ketolithocholic acid (12-keto-LCA), 3-
762 Dehydrocholic acid (3-DHCA), 6-Ketolithocholic acid (6-keto-LCA), 7-Dehydrocholic acid (7-
763 DHCA), 7-Sulfocholic acid (7-sulfo-CA), Allocholic acid (ACA), Cholic acid-7ol-3one (CA-
764 7ol-3one), Ursocholic acid (UCA), Dehydrolithocholic acid (DHLCA), Hyodeoxycholic acid
765 (HDCA), Murideoxycholic acid (MDCA), Ursodeoxycholic acid (UDCA).

### *Targeted short-chain fatty acid measurement*

For the quantitation of short-chain fatty acids (SCFAs) the 3-NPH method was used [86]. Briefly, 40 µL of the fecal extract and 15 µL of isotopically labeled standards (ca 50 µM) were mixed with 20 µL 120 mM EDC HCl-6% pyridine-solution and 20 µL of 200 mM 3-NPH HCL solution. After 30 min at 40°C and shaking at 1000 rpm using an Eppendorf Thermomix (Eppendorf, Hamburg, Germany), 900 µL acetonitrile/water (50/50, v/v) was added. After centrifugation at 13000 U/min for 2 min the clear supernatant was used for analysis. The same system as described above was used. The electrospray voltage was set to -4500 V, curtain gas to 35 psi, ion source gas 1 to 55, ion source gas 2 to 65 and the temperature to 500°C. The MRM-parameters were optimized using commercially available standards for the SCFAs. The chromatographic separation was performed on a 100 × 2.1 mm, 100 Å, 1.7 µm, Kinetex C18 column (Phenomenex, Aschaffenburg, Germany) column with 0.1% formic acid (eluent A) and 0.1% formic acid in acetonitrile (eluent B) as elution solvents. An injection volume of 1 µL and a flow rate of 0.4 mL/min was used. The gradient elution started at 23% B which was held for 3 min, afterward the concentration was increased to 30% B at 4 min, with another increase to 40%B at 6.5 min, at 7 min 100% B was used which was hold for 1 min, at 8.5 min the column was equilibrated at starting conditions. The column oven was set to 40°C and the autosampler to 15°C. Data acquisition and instrumental control were performed with Analyst 1.7 software (Sciex, Darmstadt, Germany). SCFAs measured are Acetate, Propionate, Butyrate, Valeric acid, Desaminotyrosine and the Branched-chain Fatty acids (Isobuytirc acid, 2-Methylbutyric acid and Isovaleric acid).

## Transfer experiment

Mice were gavaged with cecal microbiota at CT13 from either *Bmal1*$^{IEC-/-}$ or their controls (n=4, mixture) into germ-free wild type C57BL6 recipient mice. 100µl of 7x10$^6$ bacteria/µl were used for gavaging each mouse. Mice were weekly monitored for bodyweight changes and feces was

sampled over 24h at week 5 after gavage in DNA stabilizer. Mice were sacrificed on second day of DD at CT13.

### *Immune cell isolation from the lamina propria*

Immune cells were isolated from freshly isolated jejunum and colon. Intestinal tissues were flipped, washed out and cut into 1 cm pieces. To remove epithelial cells, pieces were incubated in DMEM with 20 µL of 1M DTT. After shaking for 15 minutes, tissues were incubated in PBS with 200 µL of 150mM EDTA at 37°C with shaking. Jejunum tissue was then digested at 37°C for approximately 10 min in a shaking incubator with 0.6 mg/ml type VIII collagenase (Sigma-Aldrich). Colonic tissue was digestion at 37°C for approximately 15 min in a shaking incubator with 0.85 mg/ml type V collagenase (Sigma-Aldrich), 1.25 mg/ml collagenase D (Sigma-Aldrich), 10µl/ml Amphotericin (100x) 1 mg/mL Dispase II, and 10 U/µL DNase-V (Sigma). Following digestion, intestinal cells were passed through a 40 µm strainer. Consequently, cells were fixed with 2% PFA, washed, and stored in RPMI at 4 °C until further processing.

### *Fluorescence-activated cell sorting (FACS)*

For intracellular stainings, cells were permeabilized with saponin 0.5% and stained with anti CD8 PE-, anti CD3 PerCP/Cy5.5, anti CD4 FITC-, anti IL-17a PE/cy7-, anti INFy- APC conjugated antibodies at dilution 1/100-1/50 for 30 min.

Surface stainings were performed using anti CD11c PE-, anti CD11b APC Cy7-, anti F4/80 PE/cy7-, anti Ly6G APC conjugated antibodies at dilution 1/50 for 30 minutes. Cells were analyzed on a LSR-II (BD Biosciences) flow cytometer and analysis was performed using FlowJo software (FlowJo, LLC).

### *Histology*

In formalin fixated tissues in paraffine were cut into 5 µm thick slices and consequently stained according to the following steps: xylene/ 5 min, xylene/ 5 min, Ethanol 100%/ 5 min, Ethanol 100%/ 5 min, Ethanol 96%/ 2 min, Ethanol 96%/ 2 min, Ethanol 70%/ 2 min, Ethanol 70%/ 2

min, Water/ 30 s, hematoxylin/ 2 min, tap water/ 15 s, Scotts Tap Water/ 30 s, Water/ 30 s, Ethanol 96%/ 30 s, Eosin/ 30 s, Ethanol 96%/ 30s, Ethanol 96%/ 30 s, Ethanol 100%/ 30 s, Ethanol 100%/ 30 s, Xylene/ 90 s, Xylene/ 90s (Leica ST5020 multistainer). DPX new mounting media (Merck) was added to preserve the tissues. Stained slides were scanned and further analyzed for histological scoring. Histological scores were assessed blindly based on the degree of immune cell infiltration of all colonic wall layers (mucosa, submucosa and muscularis), crypt hyperplasia, goblet cell depletion and mucosal damage, resulting in a score from 0 (not inflamed) to 12 (severely inflamed) according to Katakura method [87].

### *Immunofluorescence staining of CD3*

Antigens retrieval of the de-paraffinized and re-hydrated sections was performed by heating the slices in citrate buffer for 34 minutes. After multiple washing steps and tissues were blocked by donkey blocking buffer (1h at room temperature and 1hour at 4C). Tissue sections were incubated overnight with Anti E-cadherin (1:300, mouse, Abcam) anti-CD3 (1:400, rabbit, sigma). Tissue were washed with PBS and followed by incubation with secondary antibodies (donkey anti rabbit 546, donkey anti mouse 647, both from invitrogen with a dilution 1:200) for 1h at room temperature. Finally, DAPI (Sigma) were used to stain the nuclei and then tissues were mounted using Aquatex. Sections were visualized with Fluoview FV10i microscope (Olympus, Shinjuku, Japan).

## PICRUST 2.0

For prediction of functional of metagenomic functionality. Sequence of the gut controlled zOTUs, captured as described above, were used to construct the metagenome using PICRUST2.0 [88]. Corrected zOTU 16s rRNA gene copy number is multiplied by the predicted functionality to predicted the metagenome. Resulted enzymatic genes classified according to Enzyme Commission (EC) numbers were mapped to Metacyc pathways. Superclasses were removed and Metacyc pathways abundance was used for statistical analysis using STAMP

(2.1.3). Statistical differences were calculated based on White's non-parametric t-test and Benjamini Hochberg dales discovery rate to adjusted for multiple testing.

## Statistical Analyses

Statistical analyses were preformed using GraphPad Prism, version 9.0.0 (GraphPad Software), JTK_cycle v3.1.R ([89]) or R. With the use of the pipeline Rhea (Lagkouvardos) between-sample microbiota diversity is calculated by generalized UniFrac using GUniFrac v1.1. distances. Quantification of GUniFrac distances was always done in comparison to CT/ZT1. Circadian and diurnal patterns of individual 24h period graphs as well as phase calculation were analysed by fitting a cosine-wave equation: y=baseline+(amplitude·cos(2·π·((x-[phase shift)/24))), with a fixed 24-h period or by using the non-parametric algorithm JTK_cycle. Some CCGs were analysed with a harmonic-regression : y=baseline+(amplitudeA*cos(2·π·((x-[phaseshiftA)/24)))+(amplitudeB*cos(4·π·((x-[phase shift)/24))). Analysis between two groups was performed using the non-parametric Mann-Whitney test. A p value ≤0.05 was assumed as statistically significant.

Heatmaps were generated using the online tool "heatmapper.ca" [90]. Heatmaps were sorted based on peak phase of controls. Abundance plots were generated using SIAMCAT package in R using the "check.associations() function" [91]. Visualisation of zOTUs and samples trees were conducted using the online platform "evolgenius.info" [84]. Metabolite-microbiota correlation analyses was performed on relative abundance zOTU level within the rhythmic in male *Bmal1*$^{fl/fl}$ but not *Bmal1*$^{IEC-/-}$ samples with at least a 30% prevalence. Spearman correlation and adjusted p-values between targeted metabolomics and zOTUs were calculated using the *rcor()* function in R. Correlation matrixes were visualized within the R package "corrplot" (Wei et al., 2017). Only correlations were plotted with a P-value of <0.05 and coefficient values R ≤

865 −0.5 and ≥0.5. Furthermore, M2IA online platform [92] was used for the global similarity
866 analyses (PA plot) between metabolome and microbiota data.

# References


1. Dunlap, J.C., *Molecular bases for circadian clocks.* Cell, 1999. 96(2): p. 271-90.
2. Schibler, U., J. Ripperger, and S.A. Brown, *Peripheral circadian oscillators in mammals: time and food.* J Biol Rhythms, 2003. **18**(3): p. 250-60.
3. Duguay, D. and N. Cermakian, *The crosstalk between physiology and circadian clock proteins.* Chronobiol Int, 2009. **26**(8): p. 1479-513.
4. Zhang, R., et al., *A circadian gene expression atlas in mammals: implications for biology and medicine.* Proc Natl Acad Sci U S A, 2014. **111**(45): p. 16219-24.
5. Pacha, J. and A. Sumova, *Circadian regulation of epithelial functions in the intestine.* Acta Physiol (Oxf), 2013. **208**(1): p. 11-24.
6. Hoogerwerf, W.A., *Role of clock genes in gastrointestinal motility.* Am J Physiol Gastrointest Liver Physiol, 2010. **299**(3): p. G549-55.
7. Peterson, L.W. and D. Artis, *Intestinal epithelial cells: regulators of barrier function and immune homeostasis.* Nat Rev Immunol, 2014. **14**(3): p. 141-53.
8. Segers, A. and I. Depoortere, *Circadian clocks in the digestive system.* Nat Rev Gastroenterol Hepatol, 2021. **18**(4): p. 239-251.
9. Leone, V., et al., *Effects of diurnal variation of gut microbes and high-fat feeding on host circadian clock function and metabolism.* Cell Host Microbe, 2015. **17**(5): p. 681-9.
10. Thaiss, C.A., et al., *Transkingdom control of microbiota diurnal oscillations promotes metabolic homeostasis.* Cell, 2014. **159**(3): p. 514-29.
11. Zarrinpar, A., et al., *Diet and feeding pattern affect the diurnal dynamics of the gut microbiome.* Cell Metab, 2014. **20**(6): p. 1006-17.
12. Reitmeier, S., et al., *Arrhythmic Gut Microbiome Signatures Predict Risk of Type 2 Diabetes.* Cell Host Microbe, 2020. **28**(2): p. 258-272 e6.
13. Liang, X., F.D. Bushman, and G.A. FitzGerald, *Rhythmicity of the intestinal microbiota is regulated by gender and the host circadian clock.* Proc Natl Acad Sci U S A, 2015. **112**(33): p. 10479-84.
14. Voigt, R.M., et al., *The Circadian Clock Mutation Promotes Intestinal Dysbiosis.* Alcohol Clin Exp Res, 2016. **40**(2): p. 335-47.
15. Coleman, O.I., et al., *Activated ATF6 Induces Intestinal Dysbiosis and Innate Immune Response to Promote Colorectal Tumorigenesis.* Gastroenterology, 2018. **155**(5): p. 1539-1552 e12.
16. Lloyd-Price, J., et al., *Multi-omics of the gut microbial ecosystem in inflammatory bowel diseases.* Nature, 2019. **569**(7758): p. 655-662.
17. Turnbaugh, P.J., et al., *An obesity-associated gut microbiome with increased capacity for energy harvest.* Nature, 2006. **444**(7122): p. 1027-31.
18. Ferraz-Bannitz, R., et al., *Circadian Misalignment Induced by Chronic Night Shift Work Promotes Endoplasmic Reticulum Stress Activation Impacting Directly on Human Metabolism.* Biology (Basel), 2021. **10**(3).
19. Gutierrez Lopez, D.E., et al., *Circadian rhythms and the gut microbiome synchronize the host's metabolic response to diet.* Cell Metab, 2021.
20. Onaolapo, A.Y. and O.J. Onaolapo, *Circadian dysrhythmia-linked diabetes mellitus: Examining melatonin's roles in prophylaxis and management.* World J Diabetes, 2018. **9**(7): p. 99-114.
21. Voigt, R.M., et al., *Circadian disorganization alters intestinal microbiota.* PLoS One, 2014. **9**(5): p. e97500.
22. Aschoff, J., *Exogenous and endogenous components in circadian rhythms.* Cold Spring Harb Symp Quant Biol, 1960. **25**: p. 11-28.
23. Tourlousse, D.M., et al., *Synthetic spike-in standards for high-throughput 16S rRNA gene amplicon sequencing.* Nucleic Acids Res, 2017. **45**(4): p. e23.
24. Bowers, S.J., et al., *Repeated sleep disruption in mice leads to persistent shifts in the fecal microbiome and metabolome.* PLoS One, 2020. **15**(2): p. e0229001.

25. Kiessling, S., G. Eichele, and H. Oster, *Adrenal glucocorticoids have a key role in circadian resynchronization in a mouse model of jet lag.* J Clin Invest, 2010. **120**(7): p. 2600-9.
26. Coleman, O.I. and D. Haller, *Bacterial Signaling at the Intestinal Epithelial Interface in Inflammation and Cancer.* Front Immunol, 2017. **8**: p. 1927.
27. Wu, M., et al., *The Dynamic Changes of Gut Microbiota in Muc2 Deficient Mice.* Int J Mol Sci, 2018. **19**(9).
28. Forman, R.A., et al., *The goblet cell is the cellular source of the anti-microbial angiogenin 4 in the large intestine post Trichuris muris infection.* PLoS One, 2012. **7**(9): p. e42248.
29. Mukherji, A., et al., *Homeostasis in intestinal epithelium is orchestrated by the circadian clock and microbiota cues transduced by TLRs.* Cell, 2013. **153**(4): p. 812-27.
30. Kuang, Z., et al., *The intestinal microbiota programs diurnal rhythms in host metabolism through histone deacetylase 3.* Science, 2019. **365**(6460): p. 1428-1434.
31. Wang, Y., et al., *The intestinal microbiota regulates body composition through NFIL3 and the circadian clock.* Science, 2017. **357**(6354): p. 912-916.
32. Hardbower, D.M., et al., *Arginase 2 deletion leads to enhanced M1 macrophage activation and upregulated polyamine metabolism in response to Helicobacter pylori infection.* Amino Acids, 2016. **48**(10): p. 2375-88.
33. Biddle, A., et al., *Untangling the Genetic Basis of Fibrolytic Specialization by Lachnospiraceae and Ruminococcaceae in Diverse Gut Communities.* Diversity, 2013. **5**(3): p. 627-640.
34. Ridlon, J.M., et al., *Bile acids and the gut microbiome.* Current opinion in gastroenterology, 2014. **30**(3): p. 332-338.
35. Ericsson, A.C., et al., *Variable Colonization after Reciprocal Fecal Microbiota Transfer between Mice with Low and High Richness Microbiota.* Front Microbiol, 2017. **8**: p. 196.
36. Gundersen, M.D., et al., *Loss of interleukin 33 expression in colonic crypts - a potential marker for disease remission in ulcerative colitis.* Sci Rep, 2016. **6**: p. 35403.
37. Liu, T., et al., *NF-kappaB signaling in inflammation.* Signal Transduct Target Ther, 2017. **2**.
38. Hooper, L.V., et al., *Angiogenins: a new class of microbicidal proteins involved in innate immunity.* Nat Immunol, 2003. **4**(3): p. 269-73.
39. Mardinoglu, A., et al., *The gut microbiota modulates host amino acid and glutathione metabolism in mice.* Mol Syst Biol, 2015. **11**(10): p. 834.
40. Wu, G., et al., *Light exposure influences the diurnal oscillation of gut microbiota in mice.* Biochem Biophys Res Commun, 2018(1090-2104 (Electronic)).
41. Deaver, J.A., S.Y. Eum, and M. Toborek, *Circadian Disruption Changes Gut Microbiome Taxa and Functional Gene Composition.* Front Microbiol, 2018. **9**: p. 737.
42. Frazier, K., et al., *High fat diet disrupts diurnal interactions between REG3g and small intestinal gut microbes resulting in metabolic dysfunction.* bioRxiv, 2020.
43. Alenghat, T., et al., *Histone deacetylase 3 coordinates commensal-bacteria-dependent intestinal homeostasis.* Nature, 2013. **504**(7478): p. 153-7.
44. Caricilli, A.M., et al., *Gut microbiota is a key modulator of insulin resistance in TLR 2 knockout mice.* PLoS Biol, 2011. **9**(12): p. e1001212.
45. Wu, S.E., et al., *Microbiota-derived metabolite promotes HDAC3 activity in the gut.* Nature, 2020. **586**(7827): p. 108-112.
46. Schroeder, B.O., *Fight them or feed them: how the intestinal mucus layer manages the gut microbiota.* Gastroenterol Rep (Oxf), 2019. **7**(1): p. 3-12.
47. Bishehsari, F., R.M. Voigt, and A. Keshavarzian, *Circadian rhythms and the gut microbiota: from the metabolic syndrome to cancer.* Nat Rev Endocrinol, 2020. **16**(12): p. 731-739.
48. Tailford, L.E., et al., *Mucin glycan foraging in the human gut microbiome.* Front Genet, 2015. **6**: p. 81.
49. Carr, F.J., D. Chill, and N. Maida, *The lactic acid bacteria: a literature survey.* Crit Rev Microbiol, 2002. **28**(4): p. 281-370.
50. Gerard, P., *Metabolism of cholesterol and bile acids by the gut microbiota.* Pathogens, 2013. **3**(1): p. 14-24.

51. Beli, E., et al., *Loss of Diurnal Oscillatory Rhythms in Gut Microbiota Correlates with Changes in Circulating Metabolites in Type 2 Diabetic db/db Mice.* Nutrients, 2019. **11**(10).
52. Govindarajan, K., et al., *Unconjugated Bile Acids Influence Expression of Circadian Genes: A Potential Mechanism for Microbe-Host Crosstalk.* PLoS One, 2016. **11**(12): p. e0167319.
53. Vavassori, P., et al., *The bile acid receptor FXR is a modulator of intestinal innate immunity.* J Immunol, 2009. **183**(10): p. 6251-61.
54. Kim, M.H., et al., *Short-chain fatty acids activate GPR41 and GPR43 on intestinal epithelial cells to promote inflammatory responses in mice.* Gastroenterology, 2013. **145**(2): p. 396-406 e1-10.
55. Segers, A., et al., *The circadian clock regulates the diurnal levels of microbial short-chain fatty acids and their rhythmic effects on colon contractility in mice.* Acta Physiol (Oxf), 2019. **225**(3): p. e13193.
56. Bhutta, H.Y., et al., *Effect of Roux-en-Y gastric bypass surgery on bile acid metabolism in normal and obese diabetic rats.* PLoS One, 2015. **10**(3): p. e0122273.
57. Haeusler, R.A., et al., *Human insulin resistance is associated with increased plasma levels of 12alpha-hydroxylated bile acids.* Diabetes, 2013. **62**(12): p. 4184-91.
58. Brufau, G., et al., *Improved glycemic control with colesevelam treatment in patients with type 2 diabetes is not directly associated with changes in bile acid metabolism.* Hepatology, 2010. **52**(4): p. 1455-64.
59. Zheng, X., et al., *Hyocholic acid species as novel biomarkers for metabolic disorders.* Nat Commun, 2021. **12**(1): p. 1487.
60. Yoshimoto, S., et al., *Obesity-induced gut microbial metabolite promotes liver cancer through senescence secretome.* Nature, 2013. **499**(7456): p. 97-101.
61. Ozcan, U., et al., *Chemical chaperones reduce ER stress and restore glucose homeostasis in a mouse model of type 2 diabetes.* Science, 2006. **313**(5790): p. 1137-40.
62. Kars, M., et al., *Tauroursodeoxycholic Acid may improve liver and muscle but not adipose tissue insulin sensitivity in obese men and women.* Diabetes, 2010. **59**(8): p. 1899-905.
63. Bernstein, H., et al., *Bile acids as carcinogens in human gastrointestinal cancers.* Mutat Res, 2005. **589**(1): p. 47-65.
64. Thaiss, C.A., et al., *Microbiota Diurnal Rhythmicity Programs Host Transcriptome Oscillations.* Cell, 2016. **167**(6): p. 1495-1510 e12.
65. Narimatsu, K., et al., *Toll-like receptor (TLR) 2 agonists ameliorate indomethacin-induced murine ileitis by suppressing the TLR4 signaling.* J Gastroenterol Hepatol, 2015. **30**(11): p. 1610-7.
66. Maslowski, K.M., et al., *Regulation of inflammatory responses by gut microbiota and chemoattractant receptor GPR43.* Nature, 2009. **461**(7268): p. 1282-6.
67. Barker, N., et al., *Identification of stem cells in small intestine and colon by marker gene Lgr5.* Nature, 2007. **449**(7165): p. 1003-7.
68. Bamias, G., et al., *Intestinal-specific TNFalpha overexpression induces Crohn's-like ileitis in mice.* PLoS One, 2013. **8**(8): p. e72594.
69. Rakoff-Nahoum, S., et al., *Recognition of commensal microflora by toll-like receptors is required for intestinal homeostasis.* Cell, 2004. **118**(2): p. 229-41.
70. Valentini, M., et al., *Immunomodulation by gut microbiota: role of Toll-like receptor expressed by T cells.* J Immunol Res, 2014. **2014**: p. 586939.
71. Xiao, Y., et al., *Interleukin-33 Promotes REG3gamma Expression in Intestinal Epithelial Cells and Regulates Gut Microbiota.* Cell Mol Gastroenterol Hepatol, 2019. **8**(1): p. 21-36.
72. Dou, X., et al., *TLR2/4-mediated NF-kappaB pathway combined with the histone modification regulates beta-defensins and interleukins expression by sodium phenyl butyrate in porcine intestinal epithelial cells.* Food Nutr Res, 2018. **62**.
73. Zheng, D., T. Liwinski, and E. Elinav, *Interaction between microbiota and immunity in health and disease.* Cell Res, 2020. **30**(6): p. 492-506.

74. Metwaly, A., et al., *Integrated microbiota and metabolite profiles link Crohn's disease to sulfur metabolism.* Nat Commun, 2020. **11**(1): p. 4322.
75. Kawai, M., et al., *Intestinal clock system regulates skeletal homeostasis.* JCI Insight, 2019. **4**(5).
76. Ubeda, C., et al., *Familial transmission rather than defective innate immunity shapes the distinct intestinal microbiota of TLR-deficient mice.* J Exp Med, 2012. **209**(8): p. 1445-56.
77. Jud, C., et al., *A guideline for analyzing circadian wheel-running behavior in rodents under different lighting conditions.* Biol Proced Online, 2005. **7**: p. 101-16.
78. Li, Z., et al., *Essential roles of enteric neuronal serotonin in gastrointestinal motility and the development/survival of enteric dopaminergic neurons.* J Neurosci, 2011. **31**(24): p. 8998-9009.
79. Edgar, R.C., *Search and clustering orders of magnitude faster than BLAST.* Bioinformatics, 2010. **26**(19): p. 2460-1.
80. Edgar, R.C., et al., *UCHIME improves sensitivity and speed of chimera detection.* Bioinformatics, 2011. **27**(16): p. 2194-200.
81. Edgar, R.C., *UNOISE2: improved error-correction for Illumina 16S and ITS amplicon sequencing.* bioRxiv, 2016: p. 081257.
82. Lagkouvardos, I., et al., *Rhea: a transparent and modular R pipeline for microbial profiling based on 16S rRNA gene amplicons.* PeerJ, 2017. **5**: p. e2836.
83. Kumar, S., et al., *MEGA X: Molecular Evolutionary Genetics Analysis across Computing Platforms.* Mol Biol Evol, 2018. **35**(6): p. 1547-1549.
84. Subramanian, B., et al., *Evolview v3: a webserver for visualization, annotation, and management of phylogenetic trees.* Nucleic Acids Research, 2019. **47**(W1): p. W270-W275.
85. Reiter, S., et al., *Development of a Highly Sensitive Ultra-High-Performance Liquid Chromatography Coupled to Electrospray Ionization Tandem Mass Spectrometry Quantitation Method for Fecal Bile Acids and Application on Crohn's Disease Studies.* J Agric Food Chem, 2021. **69**(17): p. 5238-5251.
86. Han, J., et al., *An isotope-labeled chemical derivatization method for the quantitation of short-chain fatty acids in human feces by liquid chromatography-tandem mass spectrometry.* Anal Chim Acta, 2015. **854**: p. 86-94.
87. Katakura, K., et al., *Toll-like receptor 9-induced type I IFN protects mice from experimental colitis.* J Clin Invest, 2005. **115**(3): p. 695-702.
88. Douglas, G.M., et al., *PICRUSt2 for prediction of metagenome functions.* Nature Biotechnology, 2020. **38**(6): p. 685-688.
89. Hughes, M.E., J.B. Hogenesch, and K. Kornacker, *JTK_CYCLE: an efficient nonparametric algorithm for detecting rhythmic components in genome-scale data sets.* J Biol Rhythms, 2010. **25**(5): p. 372-80.
90. Babicki, S., et al., *Heatmapper: web-enabled heat mapping for all.* Nucleic Acids Res, 2016. **44**(W1): p. W147-53.
91. Wirbel, J., et al., *Microbiome meta-analysis and cross-disease comparison enabled by the SIAMCAT machine-learning toolbox.* bioRxiv, 2020: p. 2020.02.06.931808.
92. Ni, Y., et al., *M2IA: a web server for microbiome and metabolome integrative analysis.* Bioinformatics, 2020. **36**(11): p. 3493-3498.

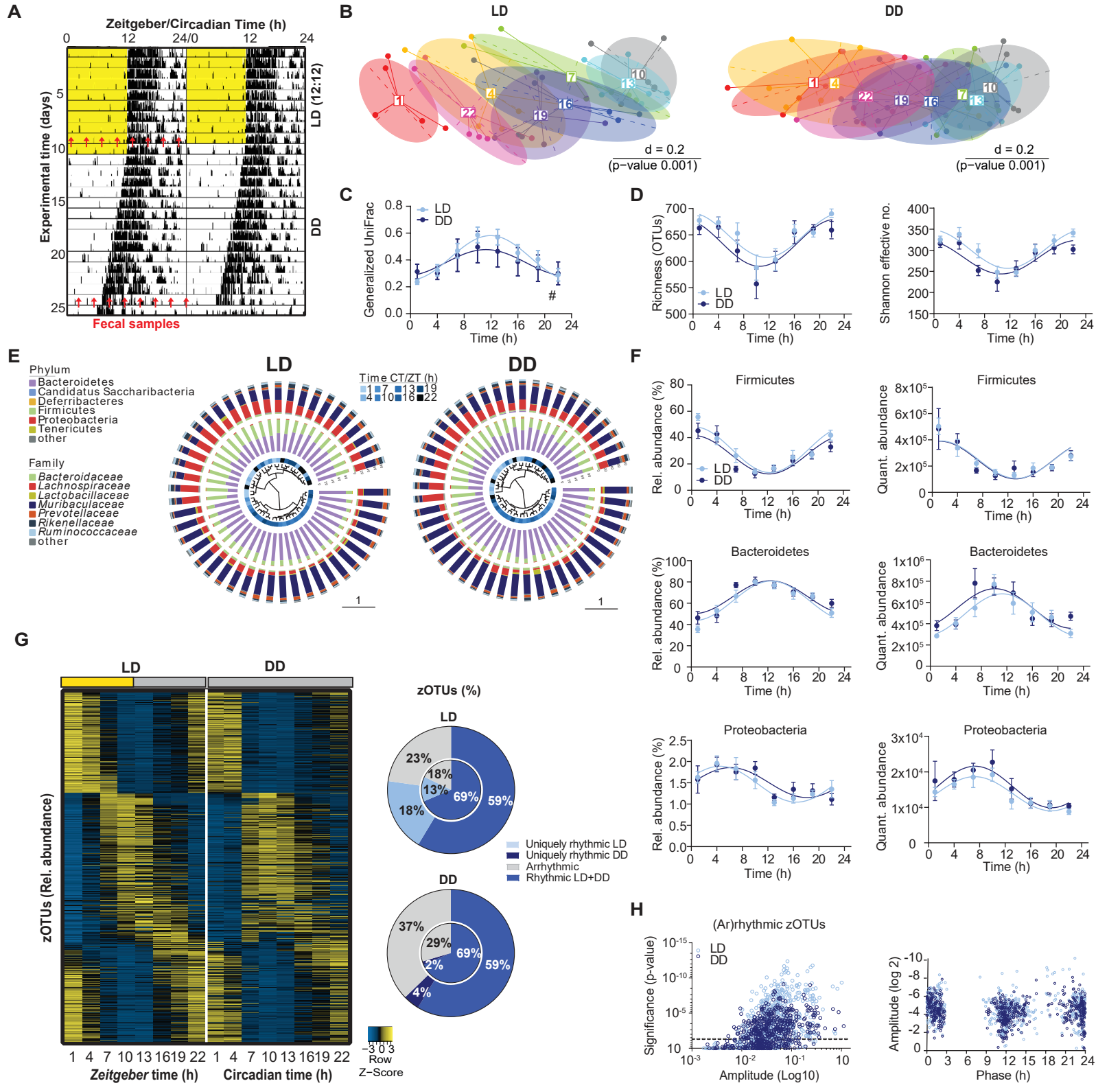
A
Zeitgeber/Circadian Time (h)
0
12
24/0
12
24
Experimental time (days)
5
10
15
20
25
LD (12:12)
DD
Fecal samples
B
LD
DD
1
4
22
19
16
7
13
10
d = 0.2
(p−value 0.001)
C
Generalized UniFrac
LD
DD
#
Time (h)
D
Richness (OTUs)
Shannon effective no.
Time (h)
E
Phylum
Bacteroidetes
Candidatus Saccharibacteria
Deferribacteres
Firmicutes
Proteobacteria
Tenericutes
other
Family
Bacteroidaceae
Lachnospiraceae
Lactobacillaceae
Muribaculaceae
Prevotellaceae
Rikenellaceae
Ruminococcaceae
other
LD
DD
Time CT/ZT (h)
1 7 13 19
4 10 16 22
F
Firmicutes
Bacteroidetes
Proteobacteria
Rel. abundance (%)
Quant. abundance
Time (h)
G
LD
DD
zOTUs (Rel. abundance)
1 4 7 10 13 1619 22 1 4 7 10 13 1619 22
Zeitgeber time (h)
Circadian time (h)
Row Z−Score
zOTUs (%)
23%
18%
13%
69%
59%
18%
37%
29%
2%
4%
Uniquely rhythmic LD
Uniquely rhythmic DD
Arrhythmic
Rhythmic LD+DD
H
(Ar)rhythmic zOTUs
Significance (p-value)
Amplitude (Log10)
Amplitude (log 2)
Phase (h)

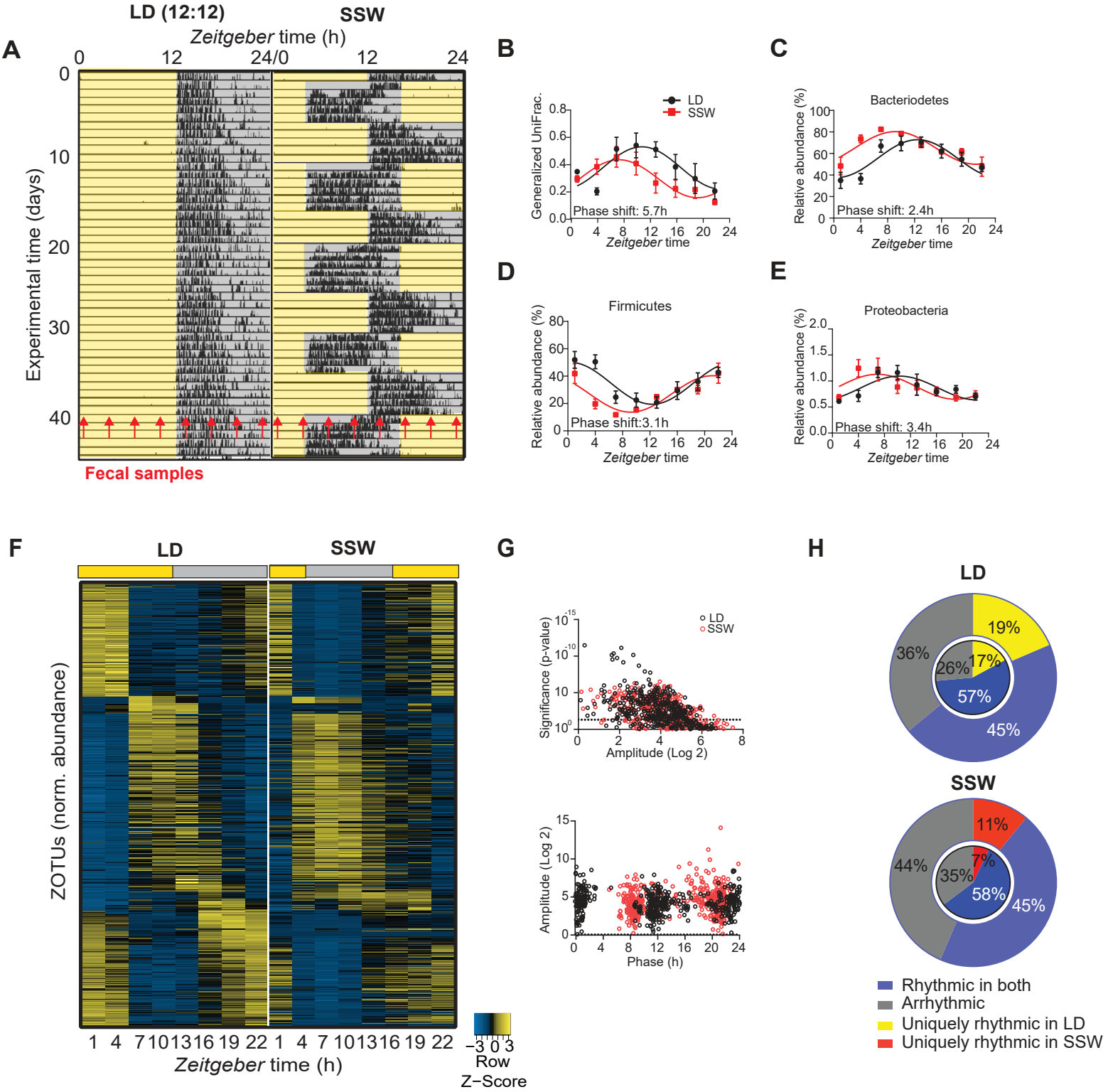
A
LD (12:12)
SSW
Zeitgeber time (h)
0
12
24/0
12
24
Experimental time (days)
0
10
20
30
40
Fecal samples
B
Generalized UniFrac.
LD
SSW
Phase shift: 5.7h
Zeitgeber time
C
Bacteriodetes
Relative abundance (%)
Phase shift: 2.4h
Zeitgeber time
D
Firmicutes
Relative abundance (%)
Phase shift:3.1h
Zeitgeber time
E
Proteobacteria
Relative abundance (%)
Phase shift: 3.4h
Zeitgeber time
F
LD
SSW
ZOTUs (norm. abundance)
1 4 7 10 13 16 19 22 1 4 7 10 13 16 19 22
Zeitgeber time (h)
−3 0 3
Row
Z−Score
G
Significance (p-value)
LD
SSW
Amplitude (Log 2)
Amplitude (Log 2)
Phase (h)
H
LD
19%
36%
26%
17%
57%
45%
SSW
11%
44%
35%
7%
58%
45%
Rhythmic in both
Arrhythmic
Uniquely rhythmic in LD
Uniquely rhythmic in SSW

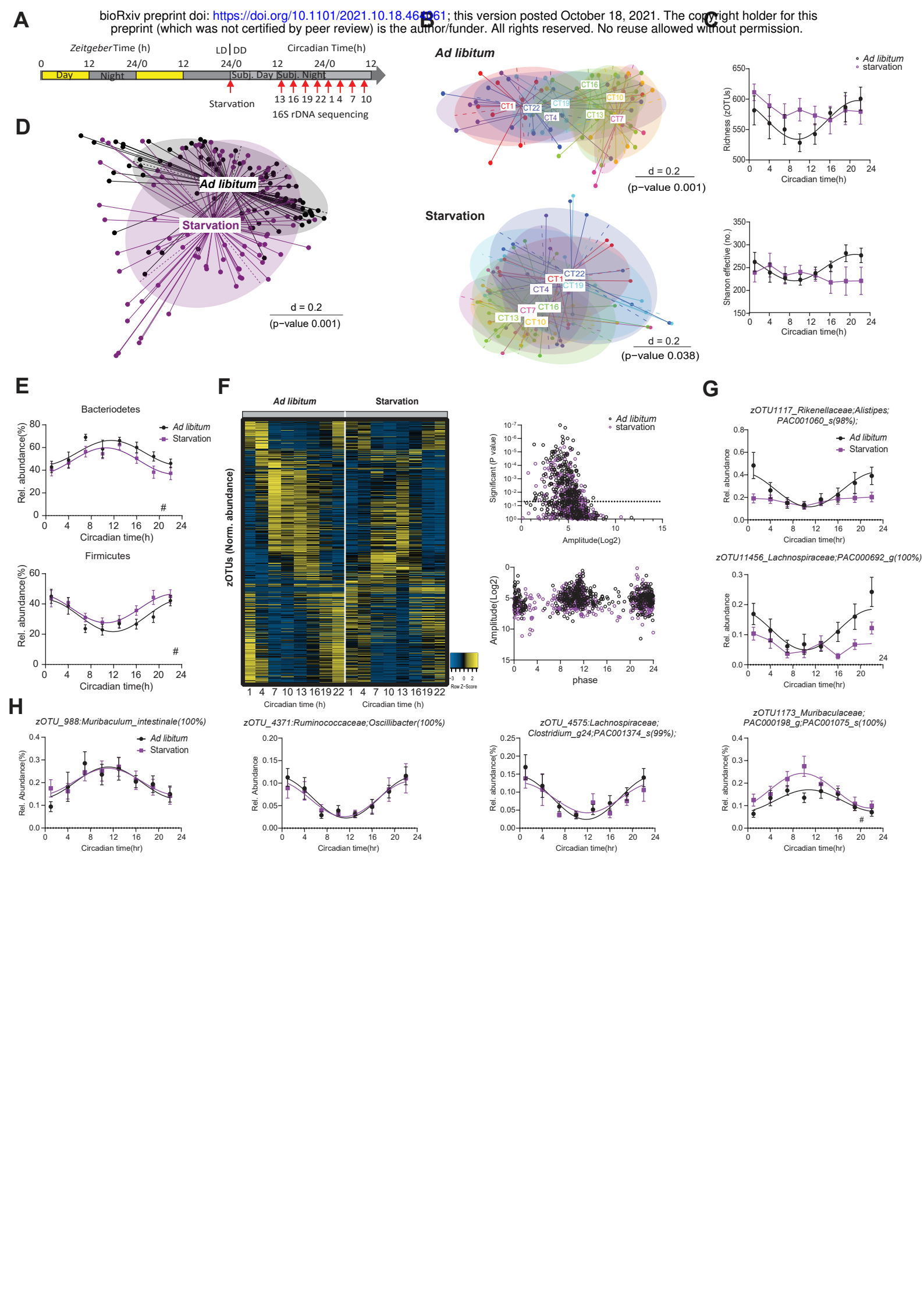

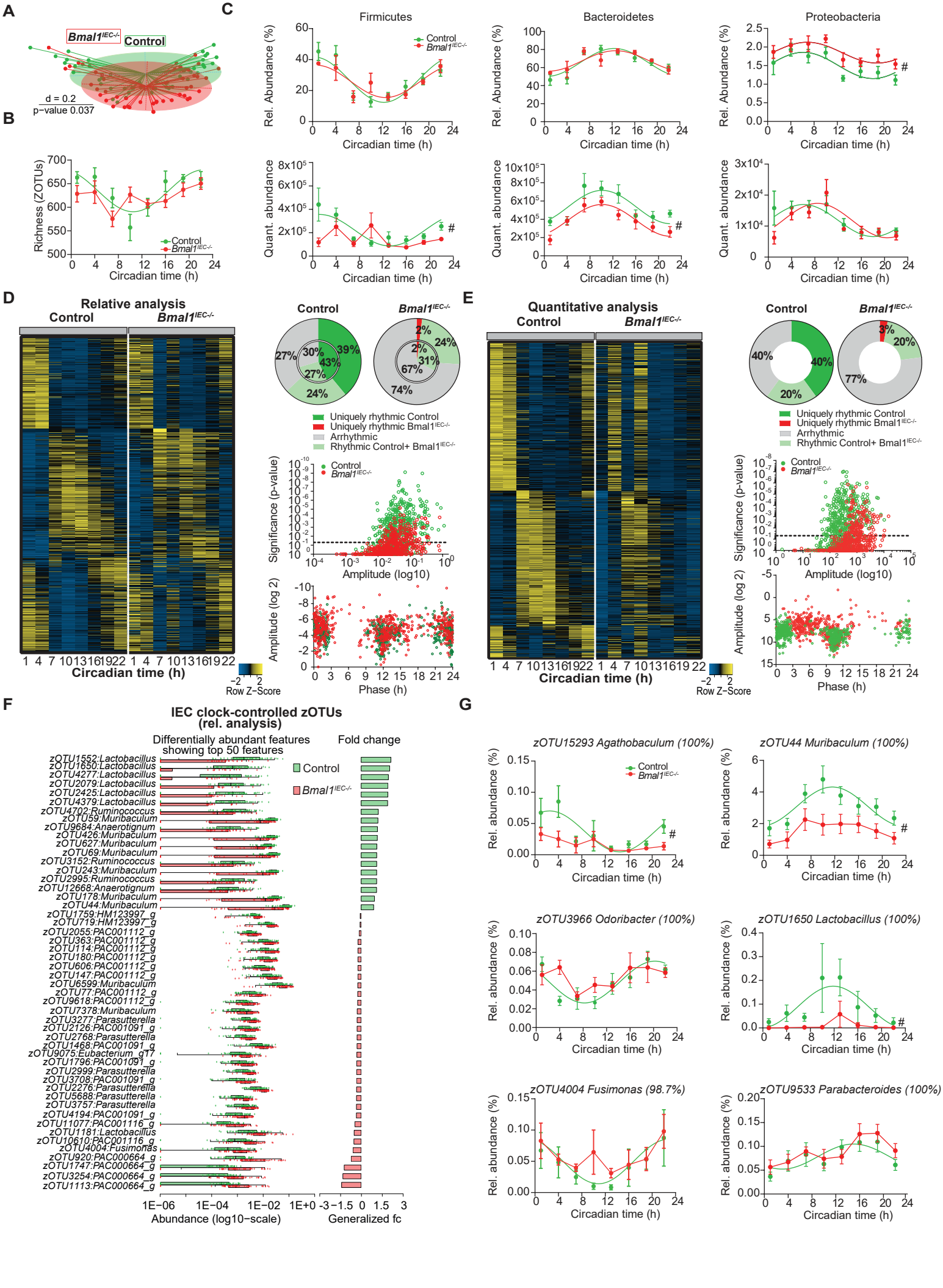

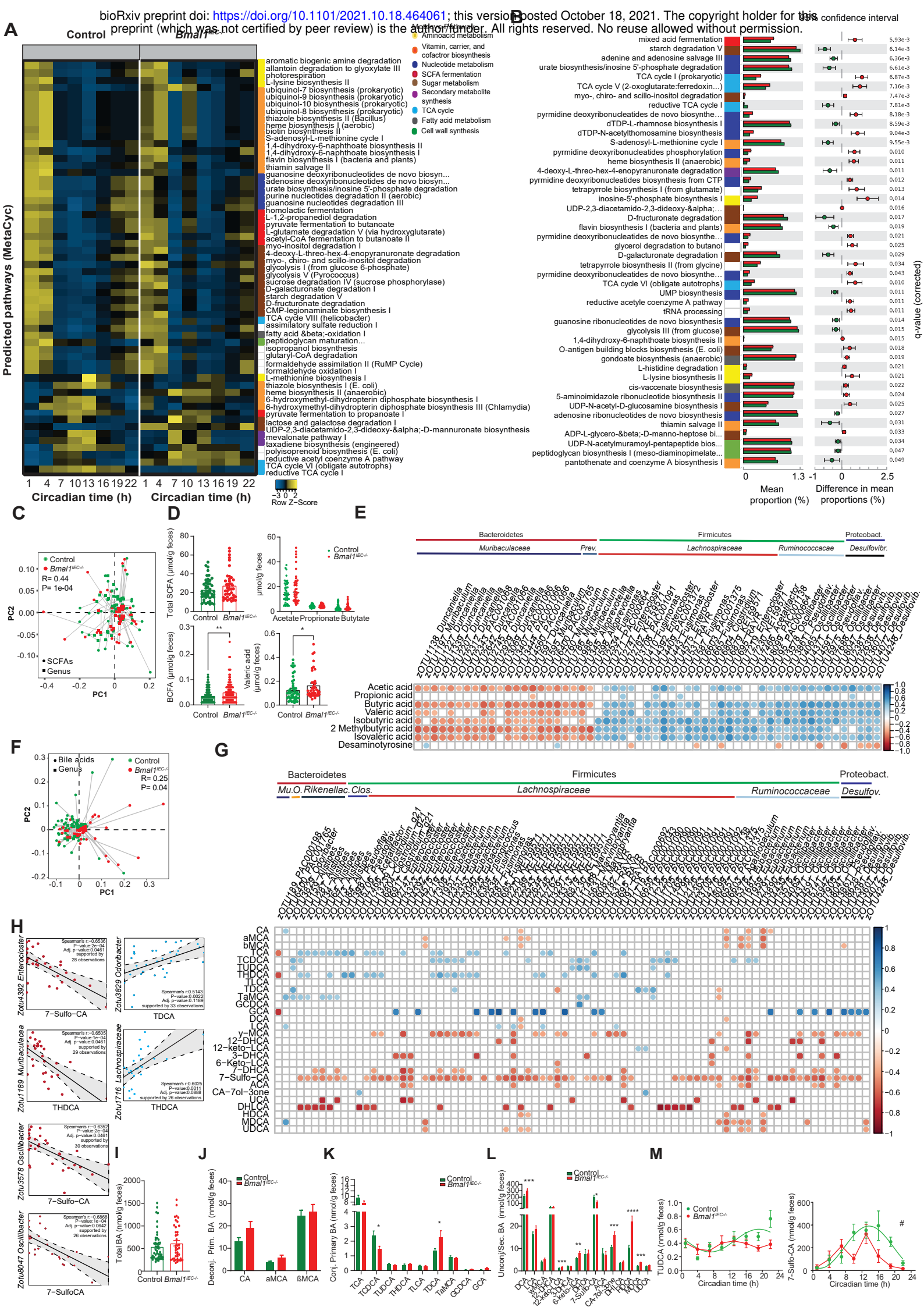

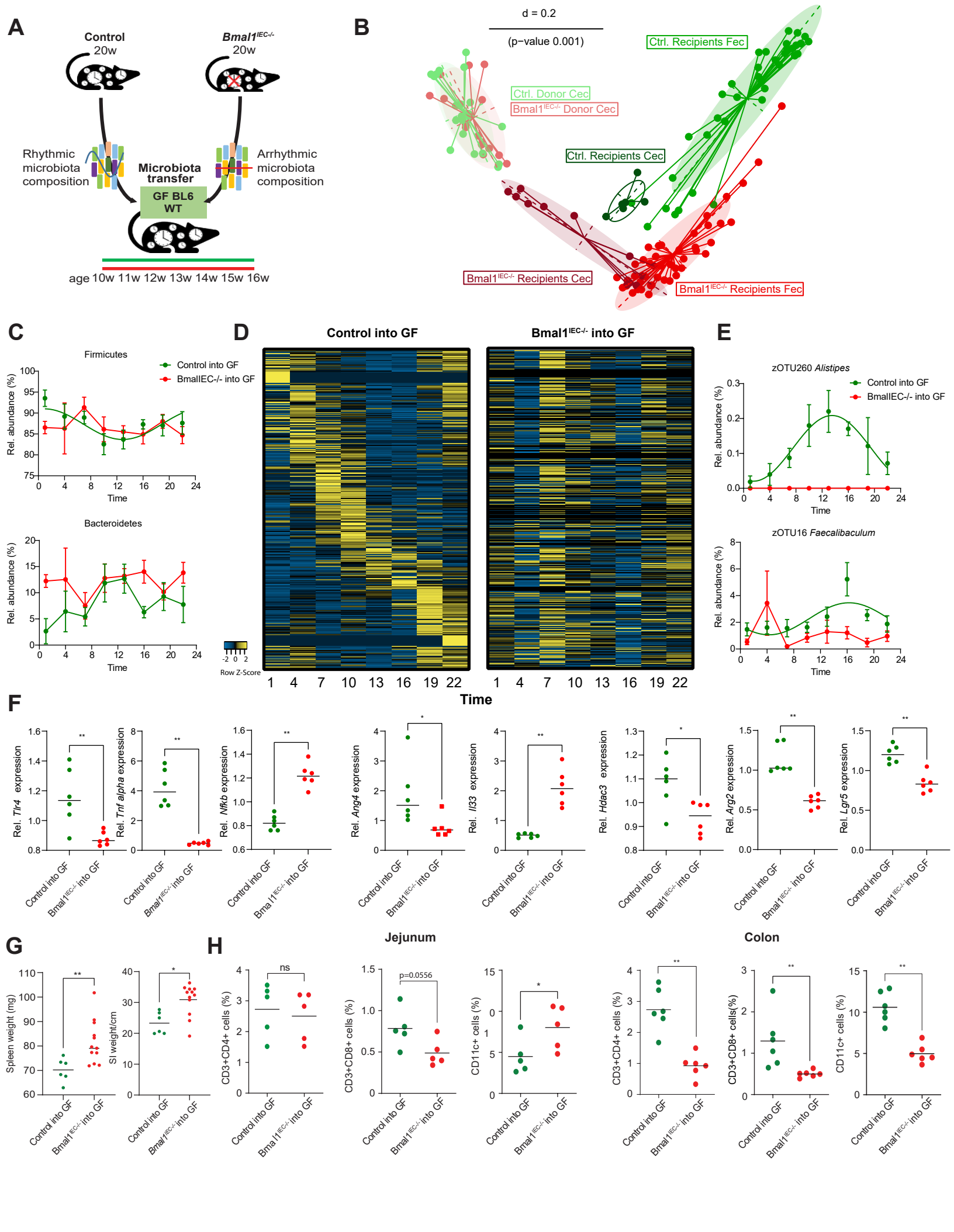
A
Control
20w
Bmal1IEC-/-
20w
Rhythmic
microbiota
composition
Microbiota
transfer
GF BL6
WT
Arrhythmic
microbiota
composition
age 10w 11w 12w 13w 14w 15w 16w
B
d = 0.2
(p−value 0.001)
Ctrl. Recipients Fec
Ctrl. Donor Cec
Bmal1IEC-/- Donor Cec
Ctrl. Recipients Cec
Bmal1IEC-/- Recipients Cec
Bmal1IEC-/- Recipients Fec
C
Firmicutes
Control into GF
BmalIEC-/- into GF
Rel. abundance (%)
Time
Bacteroidetes
D
Control into GF
Bmal1IEC-/- into GF
Row Z-Score
Time
E
zOTU260 Alistipes
zOTU16 Faecalibaculum
F
Rel. Tlr4 expression
Rel. Tnf alpha expression
Rel. Nfkb expression
Rel. Ang4 expression
Rel. Il33 expression
Rel. Hdac3 expression
Rel. Arg2 expression
Rel. Lgr5 expression
G
Spleen weight (mg)
SI weight/cm
H
Jejunum
Colon
CD3+CD4+ cells (%)
CD3+CD8+ cells (%)
CD11c+ cells (%)
CD3+CD8+ cells(%)
ns
p=0.0556